University of Nottingham
UK | CHINA | MALAYSIA

The development of novel theranostic agents for breast cancer imaging and treatment.

Sophie Duthoit.

Thesis submitted to the University of Nottingham for the degree of Masters of Pharmacy.

April 2020.

Table of Contents

Acknowledgements

I would like to thank Dr Bradshaw and Dr Turyanska for all their help and support over the last year with the practical laboratory work and writing up of my thesis, and both Amelia Hatfield and Nicola Cerioli for being fantastic lab partners. I am grateful for my mum, for encouraging me to apply for the MRes course, and for her unconditional love. Finally, I would like to thank my friends Devon, Megan, Sophie and Chloe for always being supportive and believing in me.

Abstract

Cancer is a disease that affects up to one in two people [1]. There are currently a wide variety of treatment options available but these are limited by toxic side effects such as myelosuppression and alopecia [2]. One new treatment option being developed is theranostics. Theranostics is a technique that combines therapeutic and diagnostic components, and is increasingly of interest in the field of oncology.

In my research, I am investigating the development of a theranostic compound. This compound will be 2-(4-amino-3-methylphenyl)-5-fluorobenzothiazole (5F 203) and lead sulphide (PbS) quantum dots (QDs) encapsulated in apoferritin (AFt). AFt has previously been identified [3] as an ideal drug delivery system due to its biocompatibility and non-toxicity to human cells. AFt is obtained by dialysis of ferritin (Ft), and is able to exploit the overexpressed transferrin TfR1 receptor on breast cancer cells, thus providing selectivity. The anti-tumour agent 5F 203 induces activation of the *cytochrome p450 1a1* (*cyp1a1)* gene, causing cancer cell death via the formation of DNA adducts. The effect of this compound will be studied on breast cancer cell lines MCF-7 and MDA-MB-468.

As diagnostic agents, QDs (nanoparticles with a diameter of 2-10 nm) have shown great potential for imaging. After stimulation by light absorption, they have the ability to emit at different wavelengths depending on their size. In this study, PbS QDs were investigated, which emit light in the second near infrared (NIR) close-up window between 900 and 1300 nm. QDs also have a low absorption by biological tissues and lower light scattering, resulting in deeper tissue penetration of the emitted light, and are thus show great potential for imaging.

Abbreviations

5F 203	2-(4-amino-3-methylphenyl)-5-fluorobenzothiazole
6-OH 203	2-(4-amino-3-methylphenyl)-6-hydroxybenzothiazole
AFt	Apoferritin
AhR	Aryl hydrocarbon receptor
ATP	Adenosine triphosphate
Bak	Bcl-2 homologous killer
Bax	Bcl-2 associated X-protein
Bcl-2	B-cell lymphoma 2
Bcl-X	B-cell lymphoma-extra large
BH3	Bcl-2 Homology 3
CJM 126	2-(4-aminopehnyl)-benzothiazole
CYP	Cytochrome P450
DDS	Drug delivery systems
DF 203	2-(4-amino-3-methylphenyl) benzothiazole
DLS	Dynamic light scattering
DMSO	Dimethyl sulphoxide
EMT	Epithelial-mesenchymal transition
ER	Oestrogen receptor
FBS	Foetal bovine serum
Ft	Ferritin
FWHM	Full width at half maximum
GI_{50}	Drug concentration at which cell growth is inhibited by 50%
Hepes buffer	4-(2-hydroxyethyl)-1-piperazineethanesulfonic acid
HER2	Human epidermal growth factor receptor 2
HIF-1	hypoxia inducible factor-1
Hr	Hour
hTert	Telomerase
i.v.	Intravenously
M	Mol/dm^3
MAP	Mitogen activated protein
MDA	Microtubule disrupting agent

MET	Mesenchymal to epithelial transition
Min	Minute
MMP	Matrix metalloproteinase
mPEG	Monomethoxy polyethylene glycol
MRI	Magnetic resonance imaging
MTT	3-(4,5-dimethylthiazol-2-yl)-2,5-diphenyltetrazolium bromide
NaOAc	Sodium acetate buffer
Native-PAGE	Native polyacrylamide gel electrophoresis
NIR	Near infra-red
NIR-QDs	Near infra-red quantum dots
NT_4	Tetra branched peptides
PAMAM	Polyamidoamines
PbS	Lead sulphide
PE	Plating efficiency
PEG-PLGA	Polyethylene glycol - polylactic coglycolic acid
PET	Positron emission tomography
PL	Photoluminescence
PLA	Poly (lactic acid)
PR	Progesterone receptor
QDs	Quantum dots
Rh	Hydrodynamic radius
ROS	Reactive oxidative species
S.D.	Standard deviation
SDS	Sodium dodecyl sulphate
SF	Survival fractions
T0	Time zero
TEM	Transmission electron microscopy
TF	Transcription factor
TFR	Transferrin receptor
TGI	Total growth inhibition
TNBC	Triple negative breast cancer
TSG	Tumour suppressor gene
VEGF	Vascular endothelial growth factor

Chapter 1. Introduction

1.1 Cancer biology

Cancer is a broad term for a group of diseases involving abnormal cell growth [4], or cellular transformation. It can occur as a result of genetic mutations that underpin faulty homeostatic balance. The most common types of cancers are breast and lung, with 2.09 million cases of each being reported worldwide in 2018 [4]. In the UK, there were 367,167 new cases of cancer reported in 2015-2017 [1]. Breast cancer is the fourth most common type of cancer in the UK [5] and accounts for approximately 7% of cancer deaths. 95.8% of people diagnosed with stage one breast cancer survive for longer than a year, and ~ 76% of breast cancer cases survive > 10 years [5]. The later the diagnosis, the shorter the expected survival time is.

Tumourigenesis is multistaged and proceeds over time periods that may extend to years, even decades, with evidence that multiple genetic mutations are required to form a malignant tumour [4]. Critical genetic mutations that drive tumourigenesis occur within proto-oncogenes and tumour suppressor genes (TSGs). Proto-oncogenes are genes involved in regulating cell growth and may encode growth factors, growth factor receptors, cytoplasmic signalling proteins or nuclear transcription factors. Examples of proto-oncogenes include Ras, human epidermal growth factor receptor 2 (*HER2*) and cyclin D *(CCND1/ BCL1)*.

In humans, the *Ras* oncogene family comprises of three genes: *NRas*, *KRas* and *HRas*, which encode GTPases. They are highly regulated by guanine nucleotide exchange factors and GTPase activating proteins, which control whether Ras is bound to GTP (and therefore active), or GDP (and therefore inactive). *Ras* genes are vital in the control of signalling pathways that regulate cell proliferation, cell adhesion and apoptosis. One of these pathways is the mitogen activated protein (MAP) kinase cascade, which is involved in cell growth and division. Ras proteins are also involved in activating the P13/Akt/mTor pathways which ultimately results in the stimulation of protein synthesis and the inhibition of apoptosis. However, ~20-25% of tumours have mutations in one of the *Ras* genes, and 71% of breast tumours possess mutant *Ras*

[6]. Mutations in *Ras* commonly occur at codons 12, 13 or 61, rendering the oncogene protein product permanently switched on. Constitutively active Ras proteins promote a malignant phenotype and contribute towards many of the hallmarks of cancer, including uncontrolled proliferation and sustained angiogenesis [6].

Another example of a proto-oncogene is *HER2*. The *HER2* gene encodes a protein containing an intracellular tyrosine kinase domain, and an extracellular ligand binding domain [7]. This protein is part of the human epidermal growth factor receptor (ErbB; EGFR; HER) family of proteins, containing receptor tyrosine kinases, structurally related to the epidermal growth factor receptor [8]. When mutated into a carcinogenic oncogene, *HER2* contributes to the growth of breast cancer cells *via* an increase in epidermal growth factor protein receptors.

CCND1 is also a proto-oncogene. It encodes the cyclin D1 protein, found to be mutated in 50% of breast cancer cases [9], and is part of the cyclin family. These proteins normally function as regulators of cyclin dependent kinases (CDKS). These kinases are involved in the cell cycle transition from the G1 to the S phase (Figure 2).

Proto-oncogenes are vital in the regulation of cellular growth. They become oncogenes as a result of genetic malfunctions including gene amplification, point mutation, or translocation. These mutations maintain the pro-proliferative function of the genes, but are no longer capable of responding to normal regulatory signals. For this reason, oncogene mutations are often referred to as ‘gain of function’ mutations as they result in the gene being permanently switched on, leading to constitutive gene expression, more or aberrant protein expression or constitutive protein activity. For example when mutated, Ras proteins constitutively activate the MAP kinase cascade, which is responsible for the phosphorylation and activation of downstream proteins such as the extracellular signal-regulated kinases (ERK1 and 2). The activation of these proteins ultimately alters the translation of mRNA to proteins, thus altering the regulation of translation and transcription.

TSGs play a vital role in the body, preventing tumourigenesis. Functioning TSGs work by preventing mitosis, and thus hyperproliferation [10]. Mutations in TSGs cause a

loss of gene function, resulting in unregulated cellular growth [10]. These mutations are recessive, meaning TSGs require two mutations to lose their function. One example of a TSG is *p53*. The normal role of *p53* in the body includes activation as a response to DNA damage, or oxidative stress. In the normal response pathway, p53 accumulates rapidly in stressed cells, and is phosphorylated at its N-terminal domain [11]. The N-terminal transcriptional activation domain contains many phosphorylation sites and can be considered as the primary target for protein kinases transducing stress signals. The activation of *p53* results in the activation of DNA repair, or cellular apoptosis. However if *p53* is mutated, hyperproliferation of cells possessing potentially carcinogenic mutations occurs [12].

1.2 Hallmarks of Cancer

Tumours are commonly classified as benign or malignant. Benign tumours do not invade local tissue or metastasise to distant sites within the body. For a tumour to be classed as malignant, it has to acquire the hallmarks of cancer (Figure 1). Six hallmarks were originally defined by Hanahan and Weinberg in 2000 [13]; this seminal paper was updated in 2011, adding four further hallmarks [9]. The hallmarks of cancer are:

- self-sufficiency in growth signals,
- insensitivity to antigrowth signals,
- replicative immortality,
- angiogenesis,
- tissue invasion and metastasis,
- evasion of apoptosis,
- tumour-promoting inflammation,
- avoiding immune destruction,
- deregulating cellular energetics,
- genome instability and mutation.

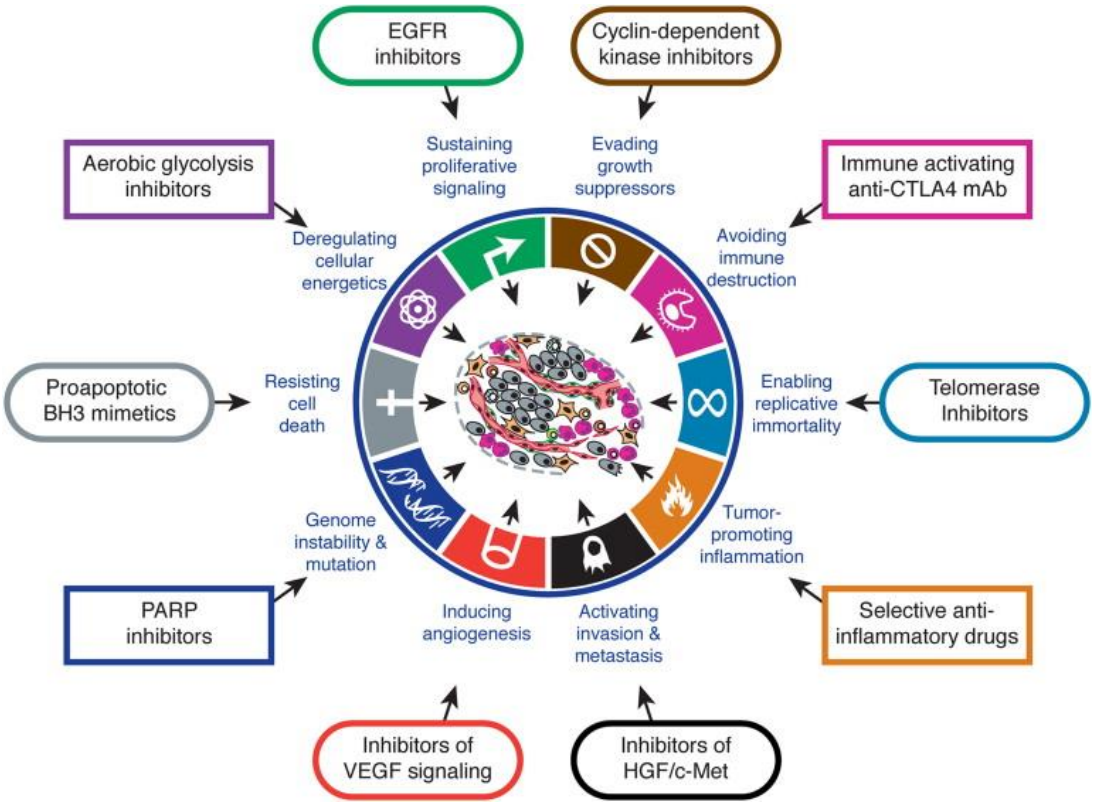

Figure 1. The Hallmarks of cancer. The ten capabilities that a tumour needs to acquire to be classified as malignant. This diagram shows therapeutic targeting options for specific cancer hallmarks. Image obtained from [9].

1.2.1 Self-sufficiency in growth signals

The normal cell cycle is shown in Figure 2 and includes the stages G1 (growth), S (DNA synthesis), G2 (growth and mitosis preparation) and M (mitosis). In the mitotic phase, separation of daughter chromosomes and cellular separation (cytokinesis) occurs [14]. During interphase, the cell may prepare to divide again.

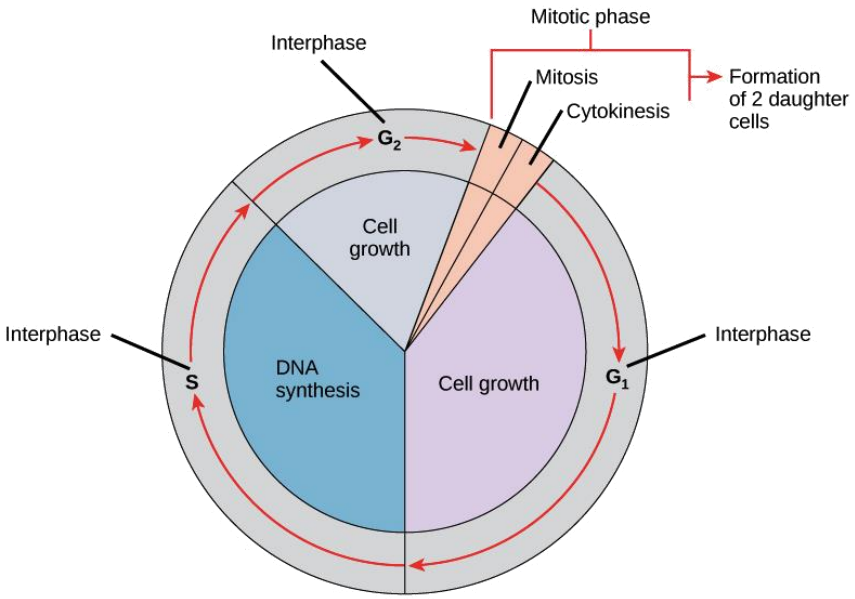

Figure 2. The cell cycle consists of interphase, mitosis and cytokinesis. Transition between the states is regulated, and cells require growth signals to progress from a quiescent to a proliferative state. Image obtained from [15].

The cell cycle is a highly regulated process, with cells requiring positive mitogenic growth signals to progress from a quiescent to proliferative state. Normally, transmembrane receptors on the surface of cells bind to signalling molecules, stimulating proliferation [16]. These signalling molecules include diffusible growth factors, extracellular matrix components and cell adhesion molecules [16]. Normal cells cannot progress from interphase to the mitotic phase without these specific signals [17]. Generally heterotypic signalling occurs, where mitogenic growth factors made by one cell type stimulate proliferation of another cell type. However, tumour cells do not require exogenous growth stimulation, meaning they are liberated from dependence on growth signals from their microenvironment. This freedom is referred to as ‘growth signal autonomy’. There are three ways in which cancer cells can obtain autonomy: alteration of extracellular growth factors, alteration of transducers of growth signals, or alteration of intracellular circuits.

Alteration of extracellular growth factors

Cancer cells can acquire the ability to synthesise growth factors to which they themselves are responsive. This creates a positive feedback loop, and results in

uncontrolled proliferation. An example of this is in glioblastomas, which secrete platelet-derived growth factor (PDGF) [18], resulting in the activation of mitosis.

Alteration of signal transducers

Another way self-sufficiency can occur is by cancer cells over-expressing cell surface receptors. At ambient levels of growth factor with a normal amount of cell surface receptors, proliferation will not be triggered. However, when cancer cells overexpress cell surface receptors this causes them to be hypersensitive to ambient levels of growth factor, resulting in the activation of growth signals [19]. In addition, overexpression of receptors can induce ligand-independent signalling, as the receptors can cluster together resulting in activation and cellular proliferation [19].

The *HER2* gene, as introduced previously, is an example of how tumours can gain self-sufficiency in growth signals *via* independent gene amplification. In breast cancer, there can be an increase of 25-50x gene copies of *HER2* [20], resulting in a 40-100 fold protein increase [20]. Overexpression of the gene, occurring in 15-30% of breast cancer cases [7], can negatively impact patient survival rate. For example, patients with more than 5 copies of *HER2* had shorter disease free survival times, and shorter overall survival times [8]. Experiments have shown that overexpression of *HER2* encourages the formation of receptor homodimers and heterodimers involving HER2 and other HER receptors, with these dimers driving PI3K/AKT and Ras/Raf signal transduction cascades.

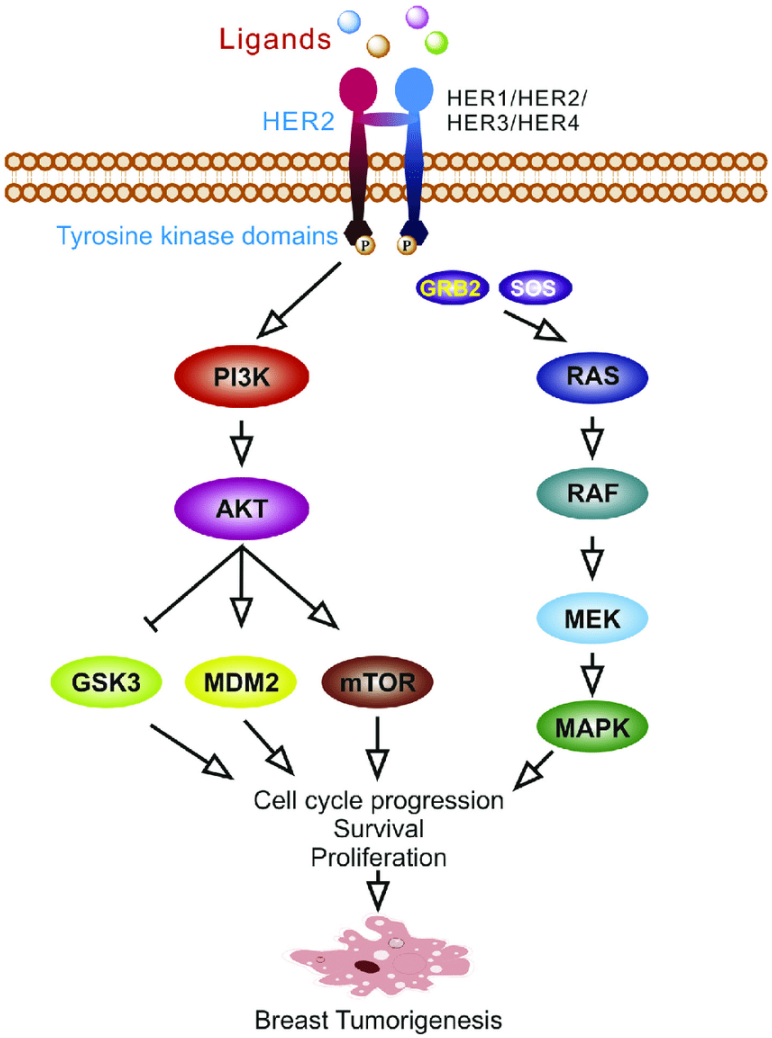

Figure 3. Her2 signalling pathways. Her2 is a receptor tyrosine kinase protein located on the cell membrane, and responds to a variety of ligands. The activation (normally *via* phosphorylation but mutated in cancer) of this tyrosine kinase domain initiates downstream signalling pathways including the PI3K/Akt pathway and the Ras/Raf pathway, resulting in tumourigenesis. Figure obtained from [21].

Alteration of intracellular circuits

Cancer cells can gain self-sufficiency in growth signals by alteration of intracellular circuits. Normally, growth factor receptors feed into the growth-promoting intracellular circuitry. The Ras-Raf-Map kinase mitogenic pathway is central to this growth signalling circuitry. However, approximately 25% of human tumours have a structural alteration in proteins in the Ras family [6], allowing mitogenic signalling without upstream stimulation. As mentioned previously, point mutations occurring in *Ras*

genes at codons 12, 13 or 61 result in constitutive activation of the Ras protein and constant signal transduction [22] .

1.2.2 Insensitivity to antigrowth signals

In normal tissue, multiple negative growth signals exist that work to maintain cellular quiescence and tissue homeostasis. These signals include both soluble growth inhibitors and immobilised inhibitors embedded in the extracellular matrix on the surface of nearby cells [17]. Antigrowth signals can cause cells to react in one of two ways. Firstly, cells can be forced to exit the cell cycle and enter the quiescent (G0) state. This is temporary, as cells can re-emerge from this state in response to positive signals. The second way antigrowth signals can affect cells is by causing them to enter a post-mitotic state known as differentiation. This is non-reversible as it causes cells to permanently lose their proliferative potential [9].

Cancer cells gain insensitivity to these antigrowth signals *via* a combination of mechanisms including chromosomal deletion, mutations, or the loss of upstream/downstream effectors. In addition, anti-growth signals can be modified directly. One of the most common anti-growth signals found to be mutated in cancer cells is the cyclin-dependent kinase inhibitor 2A (*CDKN2A*) [23]. This gene is commonly found to be methylated on the *2A* locus on chromosome 9p21, resulting in its inactivation and thus a loss of ability to act as an antigrowth signal [23].

1.2.3 Replicative immortality

Non-tumourigenic cells can divide a finite number (40-60) of times before entering senescence or apoptosis. This limit is known as the Hayflick limit and is due to the erosion of telomeres. Telomeres are distinct DNA structures found at both ends of chromosomes [24]. During the process of DNA replication, small segments of DNA within the telomeres are unable to be copied and are lost. Therefore after many divisions, the telomeres become a critical length and the cells enter senescence. It is at this point that the Hayflick limit of the cell has been reached.

Cancer cells can achieve replicative immortality by expressing telomerase (hTert). hTert is an enzyme that can add telomere repeat sequences (TTAGGG in humans) to

the 3” end of DNA strands. It is through this method that cancer cells are able to divide infinitely. Approximately 85-90% of cancer cells have this ability to synthesise high levels of telomerase throughout the cell cycle. The remaining 10-15% use the alternative lengthening of telomeres (ALT) mechanism. This process works by lengthening telomeres through homologous recombination [25].

1.2.4 Sustained angiogenesis

Angiogenesis is the growth of new blood vessels. It occurs in normal tissues, but similarly to the other hallmarks it is exploited by cancer cells to ensure their proliferation and survival [9]. New blood vessels infiltrating tumour masses also provide a means of escape for metastatic tumour cells. Angiogenesis is important for access to oxygen, nutrients and the disposal of metabolic waste/ carbon dioxide. There are two forms of angiogenesis; sprouting angiogenesis and intussusceptive angiogenesis. Sprouting angiogenesis is identified by sprouts composed of endothelial cells, and intussusceptive angiogenesis is identified by blood vessels forming through a splitting process [26]. The majority of cancer cells are able to trigger both [26].

As a tumour grows in size, inner tumour cells become further away from blood vessels causing them to be hypoxic. Hypoxia leads to the stabilisation of hypoxia inducible factor-1 (HIF-1). HIF is a transcription factor comprised of HIF-1α and HIF-1β. The former is degraded in the presence of oxygen, but stable in the absence of oxygen. Therefore, under hypoxia, the HIF-1 transcription factor is formed. The vascular endothelial growth factor (*VEGF*) gene possesses a HIF response element (HRE) on its promoter region, thus hypoxia is able to drive transcription of VEGF [9].

Thus, hypoxic tumour cells are responsible for the upregulation of angiogenesis initiators [27] VEGF and platelet-derived endothelial cell growth factor [28]. This release of growth factors causes the attraction of endothelial cells towards the tumour [27]; which causes the tumour stroma to produce matrix metalloproteinases (MMPs) [28]. MMPs are responsible for breaking down the extracellular matrix, allowing the migration of endothelial cells. These endothelial cells are then responsible for the formation of blood vessels, aided by adhesion factors such as integrin α or β [28]. MMPs are also involved in tissue invasion and metastasis, another hallmark of cancer.

1.2.5 Tissue invasion and metastasis

Tissue invasion and metastasis is arguably the most important hallmark for a malignant tumour to gain, as it is *via* this process that secondary tumours, or metastases are formed.

Cancer metastasis is the spreading of cancer cells to secondary tissues and organs. This process is composed of a number of consecutive events that must be completed in order for a tumour to successfully metastasise (Figure 4). To enable metastasis, cancerous cells must detach from the primary tumour. The main step in the detachment of cancer cells is the process referred to as epithelial-mesenchymal transition (EMT) [18]. In EMT, epithelial cells lose their apical-basal polarity and cell-cell adhesion, and gain migratory and invasive properties to become mesenchymal stem cells. Once these cells have become mesenchymal stem cells, they are able to detach from the primary tumour. Following the detachment of these mesenchymal cells from the primary tumour, these cells migrate around the body *via* the cardiovascular or lymphatic system. These cells then invade at what becomes a secondary tumour site, via a cascade of events known as extravasation. In extravasation, cancer cells adhere to and modify the endothelium, following which transendothelial migration occurs. Research has found that the extravasation of breast cancer cells is promoted by the expression of epidermal growth factor receptor ligands, including MMPs (as introduced in Section 1.2.4) [29]. Following extravasation, mesenchymal to epithelial transition (MET) occurs. In this process, cancer cells transform back into epithelial type cells, allowing for the formation of a secondary neoplasm.

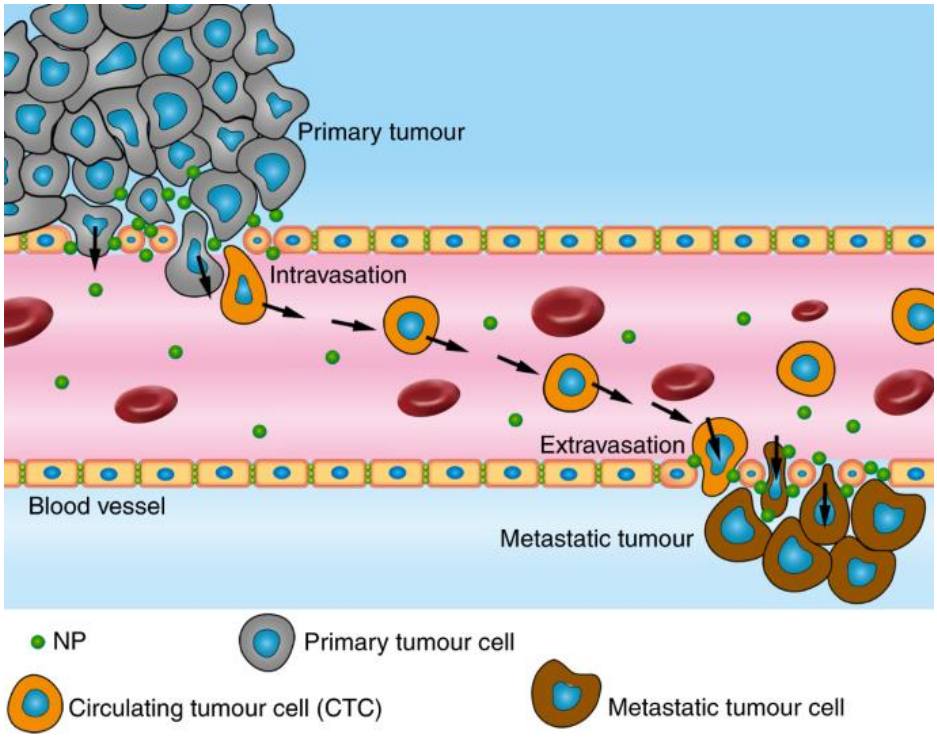

Figure 4. Tumour cells become detached through the process of EMT, following which they intravasate into the cardiovascular or lymphatic system. These cells then undergo extravasation in which MET occurs, and a secondary tumour forms. Image obtained from [30].

1.2.6 Evasion of apoptosis

Tissue homeostasis is normally maintained by the strict control and balance of cellular proliferation and apoptosis (programmed cell death) [13]. In tumourigenesis, this control is lost. Apoptosis is vital in the body, as it is used to eliminate cells that contain mutations. Characteristic features of apoptosis include membrane blebbing, nuclear fragmentation and organelle fragmentation followed by phagocytosis.

Apoptosis is initiated by either internal or external stimuli. Internal stimuli (intrinsic pathway) include abnormalities in DNA, whilst external stimuli (extrinsic pathway) may be initiated by the removal of growth factors or the addition of cytokines to a cell. Following the initiation of apoptosis, molecules known as effectors carry out the process of apoptosis. The effectors are cysteine-dependent aspartic acid-directed proteases (caspases), that degrade cellular components. Caspases exist in our cells in their inactive form of procaspases. The activation of caspases is known as a

caspase cascade, as one molecule of active initiator caspase can activate many molecules of executioner caspases. Initiator caspases include caspases 2 and 8, and executioner caspases include caspases 3 and 6.

Cancer cells are able to evade apoptosis by increasing expression of anti-apoptotic (pro-survival) genes, and decreasing expression of pro-apoptotic genes [31]. The B-cell lymphoma 2 (Bcl-2) family of proteins is an example that contains both anti- and pro-apoptotic genes. Bcl-2, B-cell lymphoma-extra large (Bcl-X) and Myeloid Cell Leukemia (Mcl-1) act as anti-apoptotic proteins, whilst Bcl-2 associated X-protein (Bax), Bcl-2 homologous killer (Bak) and Bcl-2 Homology 3 (BH3) domain molecules act as pro-apoptotic proteins [32].

Under normal conditions, following cellular stress BH3 proteins are activated, promoting oligomerisation of Bax and Bak proteins [31]. The Bax and Bak oligomers are then able to permeate the mitochondrial outer membrane, leading to cellular apoptosis [33]. Cancer cells are under constant stress due to a combination of genomic instability and cellular hypoxia [31]. Under normal conditions, this would trigger apoptosis, but cancer cells are able to avoid this cellular response by deactivating apoptotic pathways [31]. One of the ways in which they achieve this is by genetically inactivating BH3-only proteins [31].

1.3 Breast cancer

1.3.1 Incidence and mortality rate

Breast cancer is one of the most common types of malignant cancer. It is responsible for one third of cancer diagnoses [21], and one in eight women will be diagnosed with breast cancer in their lifetime [21]. The incidence of breast cancer is approximately 17,000,000 new cases (worldwide) per year [34]. Breast cancer has a mortality rate of approximately 2.4% [21]. Current evidence shows that in women younger than 45 years, breast cancer is the leading cause of cancer-related deaths [34]. One of the important factors in the treatment of breast cancer is the classification of the disease, as treatments can vary depending on the origins and molecular phenotype of the

cancer. Different types of breast cancer may be classified based on their origin as ductal or luminal. Normal breast epithelial cells are hierarchically organised broadly into bipotent mammary stem/basal (MaSC), luminal progenitor, and mature/differentiated luminal cells [22]. Figure 5 illustrates the different tissue types present in breasts.

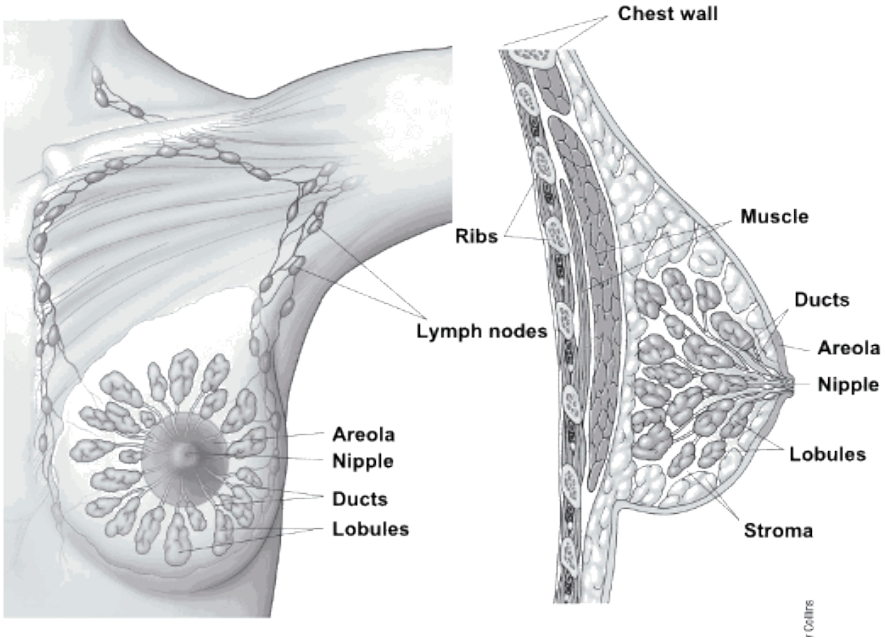

Figure 5. A diagram showing the different types of tissue present in breasts. Image obtained from [35].

1.3.2 Molecular classification of breast cancer

Historically, breast cancer was treated as a single disease. However the work by Perou and Sorlie [36] has shown breast cancer to be a heterogenous disease. There are five different classification methods for breast cancer: histological grading, tumour-node-metastasis (TNM) staging, gene expression-based signatures, genomic profile based, and network based [37]. Gene expression-based classification is most commonly used when considering treatment options, as it indicates therapies to which the tumour is likely to respond.

The main different phenotypes considered when profiling breast cancer cases are oestrogen receptor (ER), progesterone receptor (PR) and HER2 expression. ER+ refers to breast cancer that has an abundance of ER, PR+ refers an abundance of PR,

and HER2+ refers to an abundance of human epidermal growth factor receptor 2 [38]. These different tumour subtypes have different risk factors, clinical presentations and histological features, meaning treatment options vary widely. As shown in Figure 6, breast cancer demonstrating different gene-based expression have different treatment options.

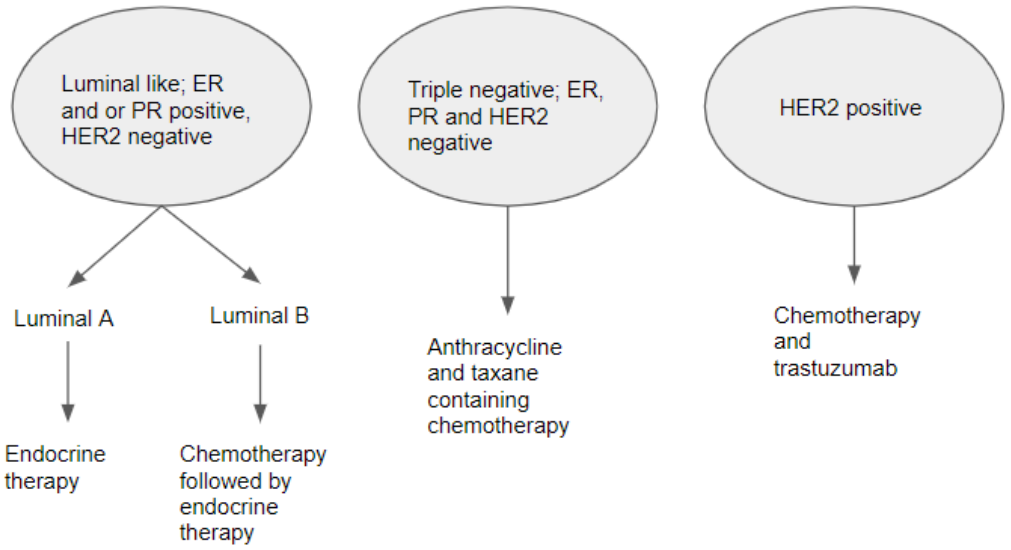

Figure 6. Diagram showing some of the common treatment options for various breast cancer types. This diagram shows how the heterogeneity of breast cancer diagnoses requires a variety of treatment options depending on the genetic mutations involved. Image adapted from [39].

1.3.3 Oestrogen receptor positive breast cancer

Approximately 80% of breast cancer diagnoses are ER+ [40]. The gene encoding the ER was named as *ERα*, due to the discovery of *ERβ* in 1996 [41]. As the role of ERβ is not well defined in breast cancer [42], when referring to ER, it is ERα being described. ERα comprises an N-terminal unstructured transactivation domain (AF1 domain) [43], a DNA binding domain, and a c-terminal ligand binding domain [29]. It belongs to a group of nuclear hormone receptors that act as transcription factors. When oestrogen binds to the ER, it translocates to the nucleus of the cell [29] where it binds to cis-regulator elements known as oestrogen response elements (EREs) [44]. This interaction is enabled by a pioneering factor (a transcription factor (TF) that can directly bind condensed chromatin) forkhead box protein O1 (FOXA1). When mutated, ERα acts as an oncogene [45]. It continues to work in its normal role as a gene-

regulating transcription factor, but an excess of ERs cause ER-mediated cell division to occur uncontrollably [46] resulting in cancer progression.

1.3.4 Progesterone receptor positive breast cancer

Approximately 65-75% of breast cancer tumours are PR+ [9]. The PR is a member of the nuclear hormone family of ligand-activated transcription factors [47]. Progesterone is normally involved in the development and regulation of hormone-responsive tissues, including the breast tissue and reproductive tract [48]. It is normally produced by the corpus luteum in the ovaries, in the second half of the menstrual cycle [47].

In PR+ breast cancer, there is an abundance of PRs present at the site of the cancer. The progesterone molecules will diffuse through the lipid membrane and interact with the hormone binding domain (HBD) [48]. Following binding, progesterone response elements in the DNA are activated, leading to the initiation of transcription of genes [48] including integrin α6, signal transducer and activator of transcription 5A (*STAT5A*) and enhancer-binding protein beta (*C/EBPβ*) [49]. The transcription of these genes promotes cell proliferation and therefore cancer growth.

1.3.5 HER2+ breast cancer

Approximately 15-30% of breast cancer diagnoses are HER2+ [50] [51]. The *HER2* gene encodes HER2 proteins, which play a role in the growth of healthy breast tissue [52]. However, in HER2+ breast cancer, *HER2* gene amplification occurs [52]. causing constitutive activation of the Ras-Raf and PI3K-AKT signal transduction cascades (as discussed earlier; Figure 3) that promote proliferation and survival of breast cancer cells [53].

1.3.6 Triple negative breast cancer

Triple negative breast cancer (TNBC) is defined as tumours that have little to no expression of ER, PR, or HER2. In the clinic, it is often identified *via* immunohistochemistry to confirm the lack of receptors [54]. It is important to confirm that the ER/PR/HER2 levels are not increased, as this limits otherwise beneficial treatment options [54]. As TNBC does not have any specific receptors that can be

targeted, it is often treated using standard or cytotoxic chemotherapy. Research has suggested that anthracycline-containing regimens are most beneficial for TNBC [55]. However, a positive diagnosis for TNBC is associated with poorer prognosis compared to other breast cancer subtypes [54] emphasising the importance of discovery and development of novel breast cancer therapies.

1.4 Current treatment options for breast cancer

Multimodal therapies are used in breast cancer treatment and include surgery, radiotherapy, anti-hormonal therapy, molecularly-targeted therapy and cytotoxic chemotherapy. The latter is a type of cancer treatment in which cytotoxic anti-neoplastic drugs are administered. It can be either neoadjuvant (delivered before surgery) or adjuvant (delivered post-surgery). Chemotherapeutic drugs (whether molecularly-targeted or cytotoxic agents) aid in treating cancer by inhibiting the hallmarks of cancer (Section 1.2); for example by inhibiting mitosis and inhibiting growth signals. Cytotoxic chemotherapy can broadly be divided into five different types (but can sometimes be subject to different classification): alkylating agents, antimetabolites, topoisomerase inhibitors, antitumour antibiotics and mitotic inhibitors.

1.4.1 Cytotoxic agents

Briefly, alkylating agents preferentially attach an alkyl group (C_nH_{2n+1}) to guanine bases in DNA, forming DNA adducts. The irreversible lesions interrupt the DNA structure and function, block DNA synthesis, resulting in cell death. As cancer cells divide more rapidly than healthy cells, they are more susceptible to the effects of the DNA damage. The most commonly used alkylating agent in the clinic is cyclophosphamide, used to treat a variety of cancers including breast, leukaemia, and ovarian cancer.

Antimetabolites either interfere with DNA base synthesis production, or are base-analogues aberrantly incorporated into DNA, thereby preventing cell division. Because of cancer cells` rapid division they are considered more susceptible to the effects of antimetabolites than `normal` cells. Antimetabolites interfere with DNA production by impairing DNA replication machinery, either by incorporation of altered nucleotides, or depletion of available deoxynucleotides. For example, in 5-fluorouracil, the fluorine

blocks in addition of the new nucleobase, resulting in the failure of DNA replication. Another example of an antimetabolite is methotrexate. This works by inhibiting dihydrofolate reductase, and preventing the production of bases required for DNA synthesis, resulting in the inhibition of the cell cycle in the G1 phase. Whilst methotrexate is a chemotherapeutic agent used in the clinic, in some adult patients it can cause cardiac symptoms and arrhythmias [56], highlighting the need for the development of drug delivery systems (Section 1.6).

Topoisomerases are enzymes that are involved in the unwinding, ligation and religation of DNA in transcription/replication. They catalyse changes in DNA topology. Topoisomerase inhibitors function either by inhibiting the enzymes` catalytic activity, or by associating with and stabilising topoisomerase-DNA complexes. Both of these methods result in the blockage of DNA transcription and replication. One topoisomerase inhibitor used in the treatment of gastrointestinal tumours is campthothecin [57]. It was discovered in 1966 during the screening of natural products, and works by stabilising the topoisomerase 1 and DNA complex.

Antitumour antibiotics work by altering cancer cells DNA, thus preventing them from growing or dividing by intercalating/ alkylating/ crosslinking DNA. One of the most commonly used antitumour antibiotics is doxorubicin, an anthracyclin antibiotic. Doxorubicin inhibits topoisomerase 2 (and therefore limits DNA synthesis), intercalates DNA double helix at G-C rich sequences, and generates ROS (reactive oxidative species).

Microtubule disrupting agents (MDAs), also termed mitotic inhibitors or mitotic spindle poisons work by disrupting microtubules that are critical for chromosome migration, mitosis and cell division. MDAs may either inhibit the formation of microtubules by inhibiting polymerisation of microtubules and causing depolymerisation of microtubules (e.g. the vinca alkaloids vincristine and vinblastine). Alternatively, MDAs may promote polymerisation of tubulin, stabilising microtubules and preventing depolymerisation of microtubules. The taxanes (including paclitaxel, originally isolated from the Pacific Yew tree *Taxus brevifolia*, and semi-synthetic docetaxel) are MDAs that stabilise microtubules. In 2015, it was concluded that chemotherapy regimens that

included taxanes improved survival and decreased the progression of metastatic breast cancer patients [58].

1.4.2 Antihormone treatments

Antioestrogens are a type of drug that inhibits the biological effects of oestrogen in the body. They work by either blocking oestrogen receptors, or inhibiting oestrogen production. Tamoxifen acts as a selective oestrogen receptor modulator, and works by competitively binding to oestrogen receptors in tumour cells.

Anti-hormone treatments used in breast cancer often target excess androgen (a type of steroid hormone that binds to androgen receptors) that is found in both ER+ and ER- breast cancer tumours [59]. In ER+ tumours, excess androgen can stimulate tumour growth following its conversion to oestrogen in tumour tissue. One of the main treatment methods for excess androgen ER+ breast cancer is antioestrogen and antiaromatase drugs that work against the result of excess androgen [59], one of which being Abiraterone. However, there is still a lack of treatments for the actual excess androgen. In ER- tumours, excess androgen can also stimulate tumour growth, by increasing the production of epidermal growth factor. This contributes towards breast cancer growth, as epidermal growth factor receptor has been found in 30% of ER- tumours [60].

1.4.3 Molecularly targeted agents

Drugs in this class predominantly include tyrosine kinase inhibitors (TKIs) [50]. Examples of drugs in this class are lapatinib and neratinib. These work by competing for the adenosine triphosphate binding domain in the cytoplasmic portion of the HER2 receptor present on the surface of cancer cells. This competitive binding prevents phosphorylation and activation of the signalling transduction pathways involved in the development of HER2 cancers [50].

Another type of dug in this category, primarily used to treat HER2 overexpression include trastuzumab and pentuzumab, pioneer antibody therapies [50]. These drugs work by recruiting innate immune effector cells to mediate tumour lysis [50].

Recent treatment advances include development of antibody-drug conjugate (ADC) therapies exemplified by trastuzumab-emtansine (Kadcyla). The humanised monoclonal antibiotic transtuzumab is covalently linked to natural product emtansine allowing the delivery of the cytotoxic antimicrotubule agent specifically to HER2+ tumour cells.

1.4.4 Antibody drug conjugates

Antibody drug conjugates are a relatively new cancer treatment, composed of an anticancer drug conjuaged to an antibody. The use of an antibody allows for the specific targeting of tumourigenic cells, meaning drugs in this category are highly specific. One example of an antibody drug conjugate is Kadcyla, that delivers the cytotoxic antimicrobial agent emtansine to HER2+ tumours.

Despite there being a variety of cytotoxic and targeted therapies being available, current chemotherapeutics also target rapidly dividing healthy cells in the body. These include hair, bone marrow, epithelia of the gastrointestinal tract and skin, which can explain some of the side effects of chemotherapy [2] such as myelosuppression and alopecia. In addition, certain breast cancer phenotypes still carry poor prognosis, such as TNBC. This has led to the need for the development of novel therapies [54]; currently under exploration are the antitumour benzothiazoles.

1.5 Discovery and development of antitumour benzothiazoles

1.5.1 Development of 2-(4-amino-3-methylphenyl)-5-fluorobenzothiazole

Benzothiazoles are a group of compounds that contain a benzene ring fused with a thiazole ring (Figure 7) [61]. Drugs developed from this possess the same scaffold, but with additions of groups such as methyl and phenyl groups. The addition of various groups changes the abilities of the molecule. Analogues containing the benzothiazole structure can have a wide range of applications, including antibacterial [62], antiviral [63], and anti-tumour activity [64]. 5F 203 was developed during a programme to

investigate the antitumour properties of benzothiazoles. It has a formula of $C_{14}H_{11}FN_2S$ (Figure 7), and a molecular weight of 258.31.

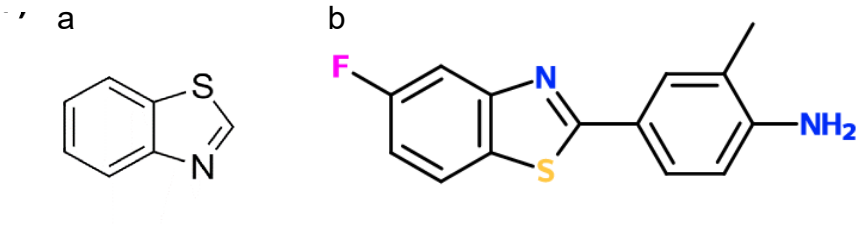

Figure 7. Chemical structure of (a) benzothiazole and (b) 5F 203. Image drawn on ChemDraw.

Antitumour benzothiazoles are ligands for the cytosolic aryl hydrocarbon receptor (AhR). Ligand binding causes translocation of the AhR into the nucleus, activating transcription of the *cyp1a1* gene [65]. This gene activation results in production of the cytochrome p450 1A1 (CYP1A1) enzyme, which metabolises the benzothiazole to a highly reactive nitrenium species capable of attacking the cells' DNA *via* adduct formation [65], resulting in single- and double-DNA strand breaks and ultimately cell death, as shown in Figure 8.

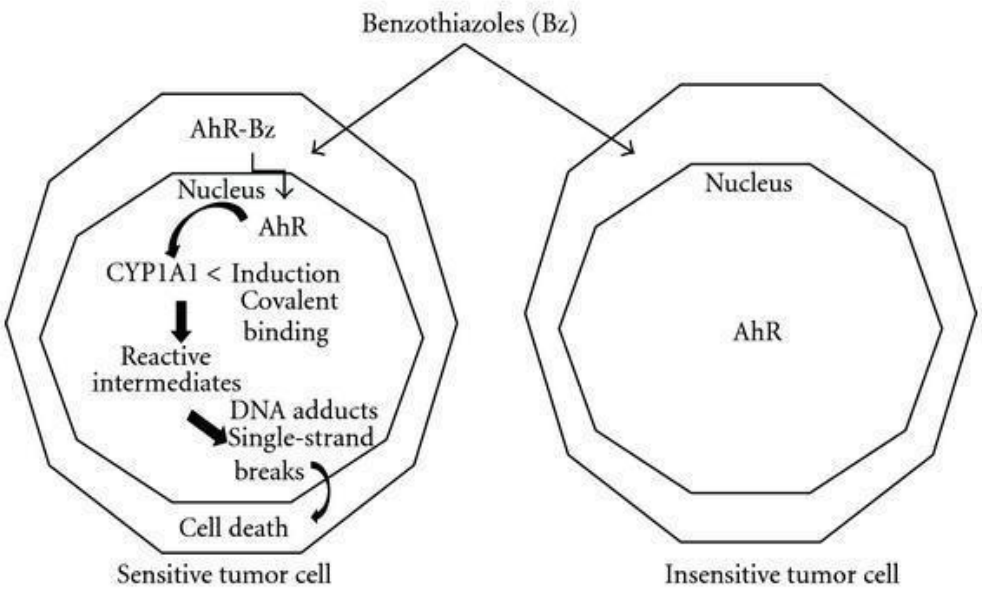

Figure 8. Benzothiazoles` mechanism of action. This diagram shows how benzothiazoles bind to cytosolic AhR receptor causing the translocation of AhR into the cell nucleus. This results in the transcription of *cyp1a1*, ultimately causing formation of DNA adducts and cellular death. Image obtained from [66].

Initially, 2-(4-aminopehnyl)-benzothiazole (CJM 126) was investigated in 1998 [64], following which analogues with enhanced potencies and extended activity spectra were synthesised. One of these analogues was 2-(4-amino-3-methylphenyl) benzothiazole (DF 203), or methylated CJM 126 [67] [68]. DF 203 was preferred over CJM 126 as it had enhanced potency, and an extended spectrum of antitumor activity both *in vivo* and *in vitro* [68].

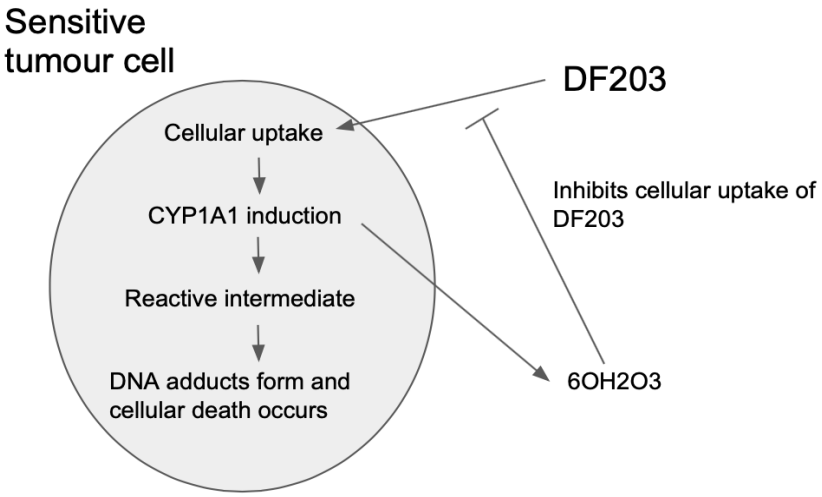

Figure 9. DF 203 mechanism of action. Cells sensitive to DF 203 have been previously found to express inducible CYP1A1 activity, which results in the production of reactive intermediates and DNA adduct formation. The DNA adduct formation results in cellular death. The production of 6OH203 was undesirable as it resulted in the inhibition of DF203 uptake and activity.

During development of DF 203, it was discovered that DF 203 was a substrate for CYP1A1-mediated metabolism and de-activation, leading to production of 2-(4-amino-3-methylphenyl)-6-hydroxybenzothiazole (6-OH 203). Figure 9 shows the mechanism of action of DF 203 leading to CYP1A1-cataysed activation and inactivation of DF 203 to electrophilic species and 6OH 203 respectively, and inactivation of CYP1A1 activity.

6-OH 2O3 inhibited the cellular uptake of DF 203, and thus limited the compound`s effectiveness. Production of 6-OH 203 resulted in an undesirable biphasic dose response. To resolve this, DF 203 was fluorinated to produce 5F 203. The fluorination at position 5 of the benzothiazole ring blocked 6-hydroxylation catalysed by CYP1A1; therefore, eradicating both the undesirable biphasic dose response and inactivating 6-hydroxylation.

1.5.2 Challenges with 5F 203

Clinical advancement of 5F 203 was limited by poor aqueous solubility and low bioavailability [69]. These issues were overcome by development of the lysylamide prodrug Phortress. *In vivo*, Phortress is hydrolysed to produce 5F 203, which can then exert the desired anti-cancer effects. In 2010, Phortress underwent phase 1 clinical evaluation. However multiple problems occurred in the trial, including recruitment of neither breast nor ovarian cancer patients. Despite this, 33% of patients experienced stable disease, including long-term stable disease in one lung, one colorectal and both renal carcinoma patients. However, patent life expired and Phortress was developed no further. Some systemic toxicities were encountered during the trial, including liver toxicity and reduced lung function, so problems to overcome included reduction of systemic exposure (and toxicity), and specific targeting of the tumour. To tackle these problems, drug delivery systems are being considered (Section 1.7.3).

1.6 Drug Delivery Systems

Drug delivery systems (DDS) were first proposed by Paul Ehrlich in 1908, and are defined as ‘engineered technologies for the targeted delivery and controlled release of therapeutic agents [70]. DDS enable the specific targeting of cancer cells, thus avoiding adverse toxicity in healthy tissues. In addition, they help prevent drug degradation and elimination by the immune system, for example by opsonins in the blood [71]. It is known that the use of drug delivery systems alters both the pharmacokinetic (PK) properties and biodistribution of a drug [70] to increase drug accumulation at the cancer site [71], and thus efficiency of treatment.

1.6.1 Passive and active targeting

Drug targeting can be classified as active or passive. Passive targeting which exploits the enhanced permeation and retention (EPR) effect, involves drug delivery of compounds directly to tumour cells. Passive targeting relies on tumour tissue characteristics, including angiogenesis/lymphangiogensis and leakage/permeability of tumour blood vessels [72]. The porous vessels and tumour architecture allow the permeation of molecules into the tumour stroma [71] [72]. In addition, impaired lymphatic drainage in tumours allows for an enhanced retention of macromolecules

(with a high molecular weight) at tumour sites [71] [72]. This type of tumour targeting relies on drug characteristics (size) and tumour biology (leakage) but does not involve any specific ligands, and is therefore referred to as passive targeting. However, there are issues with passive drug delivery. The EPR results in a high interstitial pressure which may ultimately inhibit drug accumulation in a tumour [72]. Active targeting utilises a molecular targeting agent (such as an antibody or affibody) to target tumour specific antigens such as Her2. Active targeting is generally preferred over passive, as it is less likely to produce side effects, and is able to be targeted to specific cancer sites in the body [71].

1.6.2 Drug delivery systems

Polymers are some of the most commonly used drug delivery systems. They are materials made of long repeating chains of molecules, and can be naturally occurring or synthetically made. Polymer-drug conjugations have been found to have improved solubility in aqueous medium, and a longer circulation half-life in comparison to free drugs [71]. An example of a polymer used in drug delivery is PEG-PLGA (polylactic coglycolic acid) docetaxel. PEG-PLGA encapsulated doxetaxel is also known as BIND-014, and showed promising results in clinical trials [73]. Docetaxel is a cytotoxic chemotherapeutic agent that targets all dividing cells in the body (as explained in Chapter 1.4). Delivering docetaxel in a DDS can help minimise toxic side effects in the body, as the cancer cells will be specifically targeted. The use of the PLGA polymer as a drug delivery system is combined with PEG (a compound that can coat drug delivery vehicles to enhance circulation time [74] by shielding the surface from aggregation and phagocytosis) thus prolonging circulation time [75]. Using PEG-PLGA as a drug delivery system for docetaxel results in advantages including controlled biodistribution and targeted tumour accumulation [76].

Similarly to polymers, dendrimers are also made up of repeating units. They are highly branched [77] three dimensional globular units [71] measuring 2-10 nm [71] [77], with internal cavities for the encapsulation of hydrophobic molecules. The first kind of dendrimers synthesised were polyamidoamines, or PAMAM dendrimers [78], which have been used in the clinic to increase the solubilisation of methotrexate [78]. When conjugated via ester linkages with folic acid (to selectively target folate receptors

expressed by cancer cells (Section 1.6.1)), PAMAM methotrexate was found to be fourfold more effective at killing tumour cells, in human epidermoid carcinomas [79]. Benefits of using dendrimers as a DDS include the presence of various tailorable surfaces on the dendrimers [71]. This makes it possible to attach ligands for specific tumour cell receptors. In parallel with polymers, dendrimers can also be coated in PEG, which decreases opsonisation (the marking of molecules for degradation by antibodies), and reticuloendothelial update, therefore increasing drug circulation time [71].

Similarly to dendrimers, polymeric micelles also have a hydrophobic core that can be used to encapsulate hydrophobic drugs. Polymeric micelles (aggregates of molecules in a colloidal system) are amphiphilic (containing both hydrophobic and hydrophilic parts) block copolymers, ranging in size from 20 nm to 100 nm [71]. These molecules have previously been used to encapsulate the cancer drug curcumin. Curcumin is encapsulated within the hydrophobic core of cholesterol modified monomethoxy polyethylene glycol (mPEG) poly (lactic acid) (PLA), also known as mPEG-PLA-Ch [76]. Research has found that curcumin encapsulated in mPEG-PLA-Ch exhibits higher toxicity than free curcumin in both human breast cancer and murine melanoma models [76].

Whilst dendrimers and polymeric micelles have hydrophobic cores, polymersomes have hydrophilic cores. Similarly to polymeric micelles, polymersomes are artificial vesicles made from amphiphilic block copolymers. The copolymers in polymersomes form a hollow sphere with a bilayer membrane, in which drugs can be encapsulated. One polymersome that has been used as a drug delivery system is PEGylated gelatin [71]. PEGylated gelatin-doxorubicin (PGD) was found to significantly inhibit tumour growth in comparison to free doxorubicin, in squamous cell carcinoma murine lines [76].

Another drug delivery system with a similar structure to polymersomes is liposomes [80]. Liposomes are spherical shaped bilayer vesicles, formed from phospholipid

molecules [71]. One example of a liposomal based DDS used clinically is Doxil, or PEGylated liposome-encapsulated doxorubicin (as introduced in Section 1.4.1). Encapsulating doxorubcin in the liposome allows for the limitation of cardiotoxicity in the treatment of ovarian cancer.

Proteins can also be used as DDS. Advantages associated with protein DDS include their species-specificity, non-immunogenicity, they are also biodegradable contributing to overall biocompatibility and non-toxicity; additional benefits include water solubility and uniform size [81]. There are also various moieties which can allow for tailored drug binding, or specific (molecular) targeting [82], such as the conjugation of protein subunits to antigen-specific molecular targeting affibodies. Protein materials used as DDS include keratin, collagen, elastin and silk [81]. Collagen, a main structural protein accounting for 30% of vertebrae body protein is one of the main proteins commonly utilised for optimised drug delivery [83]. An example of a protein based nanoparticle drug delivery system, pertinent to this study is AFt.

1.7 Apoferritin as a drug delivery system

1.7.1 Ferritin - an iron storage protein

Iron is an important mineral found in every cell in the human body. It is involved in many processes including oxygen transport, DNA synthesis and electron transport [84]. Specifically in oxidative phosphorylation (in adenosine triphosphate (ATP) production in mitochondria), iron is present in the iron-sulphur clusters and heme groups of the electron transport chains that allow for the generation of a proton gradient, resulting in ATP synthesis *via* ATP synthase [85]. Iron in the body must be regulated properly as an excess can form free radicals, leading to adverse effects including metabolic acidosis and liver failure [86].

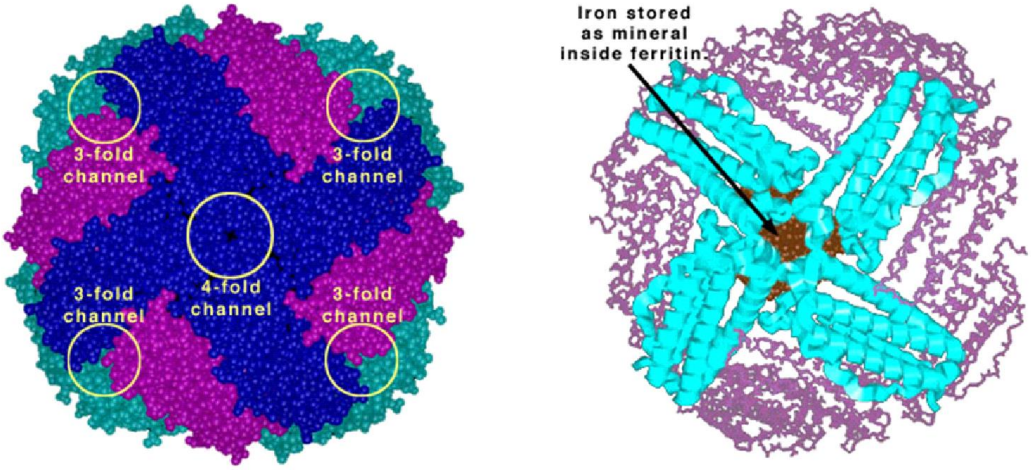

Figure 10. The quaternary structure of Ft, a hollow globular protein. There are 12 heavy and 12 light subunits that assemble to form the protein. Three-fold and four-fold channels are formed that allow the iron to leave the Ft structure. Images obtained from [87].

In the body, iron metabolism is regulated by the hepcidin-ferroportin axis [88]. Approximately half of the iron in the body is stored in the haemoglobin in the blood, and half as Ft in all cells (each Ft molecule can store up to 4500 iron ions). Ft consists of an AFt protein shell (Figure 10) and iron core, and is incorporated into haem and Fe-S cluster proteins [89].

Transferrin receptors (TFRs) are utilised for iron uptake by cells from the bloodstream. Transferrins are iron-binding blood plasma glycoproteins that regulate the level of free iron (Fe) in biological fluids [90]. There are two subtypes of TFR, TFR1 and TFR2. TFR1 is ubiquitously expressed on the surfaces of many cell types, whereas TFR2 is only expressed by liver cells [88]. TFRs sequester both transferrin-bound and Ft (AFt-encapsulated iron) from the blood. These molecules bind to TFRs, and enter the cell through clathrin-coated pit-mediated endocytosis. Therefore, as Ft is recognised by TFRs, AFt offers an ideal biocompatible molecule for drug delivery, as it would be recognised by TFRs present on (cancer) cell surfaces.

TFR1 has been found to be expressed at abnormally high (upregulated) levels in a variety of cancers [88], and is involved in the proliferation and metastasis of cancer cells [88]. These increased levels are due to enhanced iron demand associated with increased levels of cellular growth and metabolism in cancer cells. In addition, enhanced expression of TFRs is triggered by hypoxia in tumours (section 1.2.4).

1.7.2 Apoferritin encapsulation of anticancer agents

AFt (Ft without the presence of iron) is a globular protein complex comprised of 24 protein subunits that form a nanocage. It has been identified as a useful tool for drug delivery, as it has an internal diameter of 8 nm ideal for encapsulating anticancer therapeutic or imaging agents [91]. AFt has previously been used to encapsulate the cancer drugs gefitinib [92] and temozolomide [93]. AFt has also been used to encapsulate doxorubicin [3], to reduce cardiotoxicity. The use of AFt would mean that cancerous cells would be targeted via their excess TFR1 receptors, meaning lower concentrations of doxorubicin would be able to be administered. This would enable minimisation of systemic exposure, therefore limiting the effect on healthy cells in the body.

1.7.3 Apoferritin encapsulation of 5F 203

Due to the limitations such as systemic toxicity of Phortress in clinical trials (Section 1.5.2), AFt is being investigated as a DDS for 5F 203). Previous research has been carried out to optimise the encapsulation of 5F 203 inside AFt [80]. There are different methods of encapsulation that can be used, and these can be divided into nanoreactor/diffusion encapsulation, or reassembly encapsulation. In nanoreactor encapsulation, molecules are encapsulated by passive diffusion through 3 and 4 Angstrom (Å) channels at the AFt protein subunit junctions. In encapsulation *via* reassembly, AFt is dissembled into subunits, and the reassembly of the capsule is used to trap cargo. The two triggers used for reassembly are pH levels, and urea concentration.

1.8 Theranostics

Theranostics was a term coined by Funkhouser in 2002 [94], and is the process of simultaneously diagnosing and treating medical conditions. Theranostic agents aid in drug delivery and the monitoring of treatment response [95], as they provides deeper understanding of the tumour, including cellular phenotypes and heterogeneity [94]. This allows for the monitoring of specific chemotherapy effects, such as imaging tumour shrinkage [94].

Different imaging methods commonly used in the clinic include positron emission tomography (PET), magnetic resonance imaging (MRI), and optical imaging (OI) [96]. These imaging techniques can be categorised into ionising and non-ionising radiation techniques. Ionising techniques (including PET and MRI) have high sensitivity, but low spatial resolution [96], meaning they are unable to differentiate between two objects close together. Certain non-ionising radiation, such as optical imaging has the drawback of low tissue penetration. However, NIR-QDs are a type of colloidal particle that is able to emit non-ionising radiation with a deep tissue penetration.

1.8.1 Quantum dots

QDs are a type of colloidal particle (solid nanoparticles suspended in a fluid phase) [97] that possess promising qualities for imaging. They are composed of a semiconductor core, a semiconductor shell layer, and a surface layer (commonly composed of ligands including carboxyl, thiol and amine groups) (Figure 11) [98].

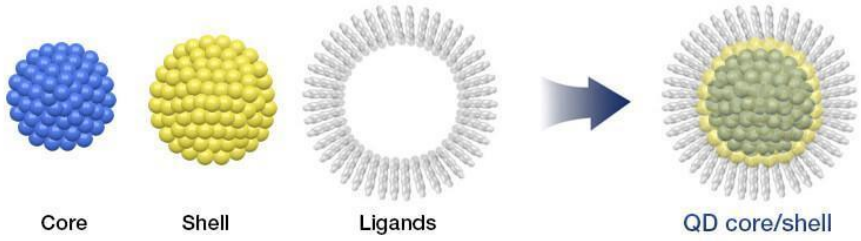

Figure 11. A figure showing the structure of QDs. Image obtained from [99].

The core material has a narrow bandgap (minimum amount of energy required to excite an electron), whilst the shell material has a higher bandgap. This difference in bandgaps confines the excitation energy to the core material [98], and results in a phenomenon known as quantum confinement. This phenomenon results in unique electronic, magnetic, mechanical, thermal and optical properties. Figure 12 shows how the composition and size of the QDs can be used to tune their optical properties to a wide range within the electromagnetic spectrum from the visible to the near-infrared wavelength range.

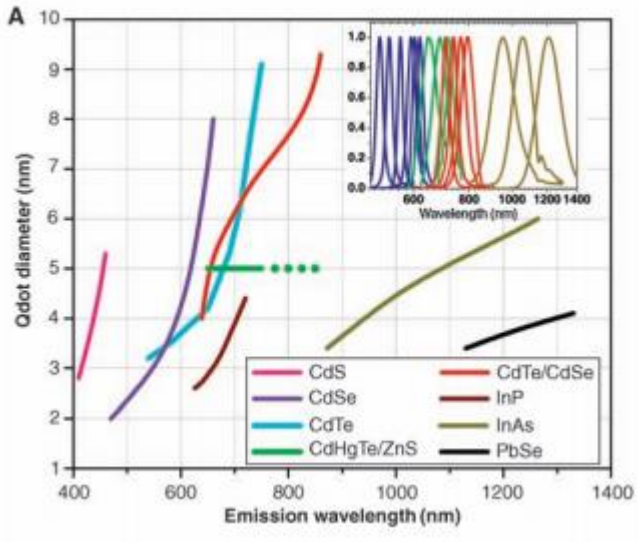

Figure 12. QDs composed of different semiconductor material have different emission wavelengths. Image obtained from [99].

QDs with emission in the near infra-red wavelength range (NIR-QDs) between 700 nm and 1300 nm are of particular interest for imaging applications. These properties include QDs have highly stable fluorescence intensity in the wavelength range of low absorption of biological tissues hence deep tissue imaging with high spatial resolution is possible. Also, there is minimal interference from background auto-fluorescence by biomolecules [100].

NIR-QDs composed of CdSe have been used previously in research, labelled with selective tetra branched peptides (NT4-QDs) to target cancer cells [100], and bound to graphene [101]. The research into NT4-QDs by Brunetti et al [100] showed NT4-QDs were much more effective at targeting cancer cells than unconjugated (free/unbound) QDs. For example, in a colon cancer mouse model there was much higher accumulation and retention of the NT4-QDs compared to the unconjugated QDs [100]. This shows that when QDs are effectively utilised they can be beneficial in cancer treatment.

1.8.2. Use of lead sulphide quantum dots in therapy

PbS QDs have demonstrated potential utility in cancer therapy. When human-derived breast cancer cell lines are exposed to AFt-encapsulated PbS QDs, concentrations ≥ 200 µg/mL triggered apoptosis [102]. In comparison, the cell cycle and viability of non-tumourigenic cells was unaltered up to concentrations of 1 mg/mL [102]. In addition to breast cancer cells, AFt encapsulated PbS QDs have also been shown to have antitumour activity in human-derived colorectal carcinoma (CRC) cells [103].

This observed cytotoxicity is potentially a result of the lead ions present that would be able to bind to the sulfhydryl groups in proteins, causing an increase in ROS [102]. In cancer cells, an increase in ROS would be more toxic (in comparison to normal cells), due to the higher metabolic rate and genetic instability of cancer cells making them more susceptible to ROS imbalance [102]. In addition, as cancer cells have increased TFR1 and decreased ferroportin, PbS delivered in AFt will be more greatly taken up and retained by cancer cells compared to non-tumourigenic cells.

Semiconductor QDs are also useful for treatment as they have small diameters (3-10 nm) [103], meaning they have longer blood circulation times, and more stable photoluminescence (PL) compared to organic dyes. In our research, we are encapsulating them within AFt to increase the circulation time and bioavailability of the compounds even further.

1.8.3 Use of quantum dots in imaging

In addition to their therapeutic benefits, QDs also have imaging benefits. The optical properties of QDs stem from their composition (chapter 1.8.1). Their specific architecture increases the PL quantum yield of the QD core, meaning that QDs are more stable, and brighter than fluorescent imaging methods [104]. In addition, the structure of QDs gives them resistance to photobleaching, meaning images can be taken for longer time periods than with fluorescent dyes [104].

Whilst groups II-VI QDs have shown potential as imaging labels and as markers in magnetic immunoassays [103], these QDs have limited uses as imaging agents as the light they emit is absorbed by biological tissues. QDs with emissions in the NIR wavelength range (1000-1350 nm) are advantageous as they have potential for deep

tissue *in vivo* imaging [103]. The NIR wavelength range can be achieved with IV-VI based semiconductor materials (eg: PbS, PbSe) [105].

One type of QD that emits light in the NIR range is PbS QDs. Previous *in vivo* research [105] has shown that AFt-PbS QDs can be used for NIR imaging in mice. The research by Zamberlan showed the production of QDs with emission in the NIR range from 920 nm to 1220 nm. QD solutions with emissions > 1000 nm were selected, to benefit from low absorption by biological tissues and lower light scattering, resulting in deeper tissue penetration of the emitted light. The research found that the use of longer wavelengths resulted in 1.5 times higher resolution than using short wavelengths, due to reduced light scattering [105].

Chapter 2. Aims and objectives

The overall aim of this project is to develop a theranostic agent by encapsulating an experimental anticancer agent (5F 203) and an imaging agent (PbS QDs) inside an AFt cage, for delivery, diagnostic imaging and treatment of breast cancer.

The specific objectives of this project include:

1. Encapsulate PbS QDs in AFt via the reassembly route, and 5F 203 in AFt via the nanoreactor/ diffusion route.
2. Characterisation via dynamic light scattering (DLS), transmission electron microscopy (TEM) and photoluminescence (PL)
3. Growth inhibitory studies

PbS QDs are encapsulated in AFt via the reassembly route, in which pH manipulation is utilised. 5F 203 is encapsulated in AFt via the nanoreactor/ diffusion route, in which channels present in AFt are utilised.

To characterise the AFt nanoparticles, DLS, TEM and PL spectroscopy are utilised. DLS (Section 3.2.1) measures the size and distribution of AFt nanoparticles. TEM (Section 3.2.3) can be used to produce images of nanoparticles, and PL (Section 3.2.4) is used to measure wavelengths and thus the sizes of nanoparticles.

To study the *in vitro* effects of both 5F 203 and encapsulated 5F 203 on cell growth and viability by 3-(4,5-dimethylthiazol-2-yl)-2,5-diphenyltetrazolium bromide (MTT), cell count and clonogenic assays. MTT assays will also be conducted to determine the effects of control vehicle DMSO and AFt drug delivery vehicle on breast cancer cell viability and proliferation. Finally, the effect of PbS QDs will be examined by MTT assay on growth and viability of breast cancer cell lines. Thereafter, MTT experiments will be performed to determine whether AFt-encapsulated PbS-5F 203 exerts enhanced activity in breast cancer cell lines. Cell count assays will be conducted to corroborate MTT assay findings. Clonogenic assays will be conducted to determine whether any observed inhibition might be as a result of cytostasis or cytotoxicity.

In developing a theranostic agent for treatment benefits, imaging features are also beneficial. Due to the presence of PbS QDs, TEM and confocal microscopy will be used to visualise intracellular AFt-cargo *in vitro* (initially) and eventually *in vivo*.

The breast cancer cell lines utilised are MCF-7 and MDA-MB-468, which represent two distinct breast cancer phenotypes: MCF-7 is a luminal A, hormone-dependent (ER+ and PR+) breast cancer cell line derived from invasive ductal carcinoma, while MDA-MB-468 is a TNBC cell line (ER-, PR-, HER2-), expressing up-regulated EGFR [106].

Chapter 3: Materials and methods

3.1 Preparation of apoferritin and encapsulation of test agents

3.1.1 Preparation of apoferritin from ferritin

To prepare AFt from Ft, the procedure previously reported by [80] was followed. A solution of horse spleen Ft (Sigma Aldrich 85 mg/mL) was diluted 10x in sodium acetate buffer (NaOAc, 0.1 M, pH 5.5). NaOAc buffer is a solution of sodium acetate and acetic acid that acts as a buffer to maintain a constant pH. Ft was then placed in a dialysis bag (MWCO 12-1400) and immersed in a solution of NaOAc buffer (0.1 M, pH 0.5, 1.5 L). Following this, the buffer was purged with N_2 for 15 mins, to eliminate oxygen from the solution and preserve the protein structure. 1mL of thioglycolic acid (0.03 M) was then added dropwise. The solution was then left under constant N_2 purge for 2h. This method was then repeated at least 5 times with new NaOAc buffer until a colourless protein sample of AFt was observed due to the iron loss from Ft. The AFt was then placed in fresh NaOAc buffer for 24 h, before being split into 1 mL aliquots and stored at -20 ^{o}C.

3.1.2 Synthesis of lead sulphide quantum dots

To synthesise PbS QDs, the method detailed in [107] was followed. To prepare the lead precursor solution, 0.364 g 0.96 mM of lead acetate trihydrate $Pb(AcO)_2 \cdot 3H_2O$ is dissolved in 60 mL of deionised water, followed by the addition of 0.52 mL (0.006 M) thioglycerol and 0.20 mL 0.002 M dithioglycerol. After this, 0.25 mL-0.58 mL of 0.1 M solution of sodium sulphide (Na_2S) was added to 5 mL of Pb-precursor solution under vigorous mixing, to form PbS QDs. The solution was then further mixed for 15 mins under N_2 flow to complete QD synthesis.

3.1.3 Encapsulation of lead sulphide quantum dots in apoferritin *via* reassembly route

PbS QDs were encapsulated *via* the reassembly method as detailed previously [107]. In the reassembly process, 5 mL of 0.09 mM AFt is disassembled into its subunits in a dialysis bag, against 150 mL of 0.1 M NaCl solution, at an acidic pH of 2. The dissembled subunits were then mixed with 5 mL of 5 mg/mL preformed PbS QDs per 5 mL of AFt stock. The pH was gradually increased to pH 5.5 by adding 0.1 M HCl, resulting in the reformation of the AFt cage with the QD captured inside. The solution was purified by dialysis to remove any un-encapsulated QDs, and by centrifugation to remove any precipitated AFt.

3.1.4 Encapsulation of 5F 203 in apoferritin *via* nanoreactor route

The nanoreactor encapsulation method relies on the passive diffusion of 5F 203 through the hydrophobic and hydrophilic channels of AFt [80].

AFt-encapsulated 5F 203 was prepared *via* the E4 N method detailed previously [80]. The AFt solution (pH 7.4, 1.0 mL, 3.2 mg/mL) was first diluted x2 in 4-(2-hydroxyethyl)-1-piperazineethanesulfonic acid (Hepes buffer; 20 mM, pH 7.4) at 4 ^{o}C. Following this, 10 mM 5F 203 dissolved in DMSO (10 mM, 0.73 µL) was added to the AFt solution at 30 min intervals until the desired number of 100 5F 203 molecules per AFt cage was achieved. The solution was then stirred for 1 h, and then dialysed (MWCO 12-1400) against Hepes buffer (20 mM, pH 7.4, 1.5 L) for 24 h. Samples were then stored at 4 ^{o}C to minimise precipitation.

3.2 Characterisation of apoferritin encapsulated nanoparticles

AFt nanoparticles can be characterised by a variety of methods including DLS, native polyacrylamide gel electrophoresis (Native-PAGE), TEM, and PL spectroscopy experiments. DLS is used to measure the size and distribution of AFt particles in the solution. It can also be used to provide information about the aggregation state of nanoparticle solutions. Native-PAGE is used to measure the size and integrity of AFt, and TEM can be used to inspect the morphological characterisation of AFt and PbS

QDs. PL spectroscopy can be used to determine nanoparticle size *via* the investigation of emitted light.

3.2.1 Dynamic light scattering

DLS is a characterisation technique that was used to measure the size and distribution of AFt particles in solution. The hydrodynamic diameter of a molecule is the size of a sphere that diffuses at the same rate as the particle being measured. Zeta potential can be defined as the potential difference between the dispersion medium and the stationary layer of fluid attached to the particle. The zeta potential indicates the stability of colloidal dispersion. A high zeta potential indicates electrical stability, whilst colloids with a low zeta potential tend to coagulate or fluctuate.

DLS works by measuring the Brownian motion of particles in a solution, which can then be used to determine the hydrodynamic size. Brownian motion is the random movement of particles that results from collisions with molecules (e.g. solvent molecules) in the solution. Smaller molecules diffuse more quickly, and larger molecules diffuse more slowly. The rate of Brownian motion can be quantified as the translational diffusion coefficient (D).

Stokes–Einstein equation is used to calculate the hydrodynamic radius Rh (the indication of how a particle moves in a fluid).

$$Rh = \frac{kT}{6\pi\eta D} \quad (1)$$

where k is Boltzmann constant, T is temperature, η is solvent viscosity.

The zeta potential describes the surface charges of the nanoparticles in suspension, and can indicate the stability of a solution. A large zeta potential from 30 mV to > 61 mV indicates a good stability, whilst values < 30 mV indicate instability. Values from 0 mV to 5 mV indicate an unstable solution where rapid coagulation or flocculation may occur.

To conduct DLS experiments, a Zetasizer Nano spectrometer (Malvern Instruments Ltd) is used at 25 °C to measure the scattered light intensity in the visible spectrum. This machine uses a 633 nm laser to analyse a 10 wt % liquid suspension of AFt. A salt solution of 10 mM NaCl was used. Samples were filtered to remove dust.

3.2.2 Native-PAGE

Protein electrophoresis is a method used to analyse the proteins present in a solution. Polyacrylamide gel electrophoresis (PAGE) is mainly used to analyse proteins and small fragments of nucleic acids. A polyacrylamide gel is preferred over an agarose gel, as polyacrylamide gels possess smaller average pore size, which is more suitable for AFt.

When analysing AFt, it is preferable to use native-PAGE over SDS-PAGE, as denaturing sodium dodecyl sulphate (SDS) should be avoided. This is because SDS would denature the secondary/tertiary/quaternary structure of the protein.

The separation of proteins depends on charge density (charge to mass ratio), size and shape of the proteins. The net charge of an overall protein depends on its pH. When conducting native-PAGE experiments, the buffer is set so all proteins at that specific pH will have a negative charge. This will cause the proteins to migrate to the anode (negative electrode). The greater the charge density of the protein, the faster the rate of migration. The extent of cross-linking in the gel and average pore size will also affect the migration of proteins. The larger the protein, the slower the migration rate. In addition, compact globular proteins migrate faster than elongated proteins of a similar molecular weight.

The method detailed in [80] was followed to analyse horse spleen AFt before and after the encapsulation of test agents. The loading buffer (50 mM Tris-HCl pH 6.8, 100 mM DTT, 50 % (v/v) glycerol, 0.1% (w/v) bromophenol blue) and the running buffer (200 mM glycine, 25 mM Tris base) were prepared. Following this, 5-10 mL of stacking gel was prepared and poured onto a gel stamp, then mixed with a quarter volume of 4x protein loading buffer lacking SDS. Thereafter, samples were loaded on the gel, and

run for 2-3 h at 125 V. The gel was stained for 30 min with Coomassie brilliant blue buffer and then de-stained for 2 h before imaging.

3.2.3 Transmission electron microscopy

TEM is a microscopic technique developed by Knoll and Ruska in 1931, used to image specimens that are too small to be viewed by optical microscopes. Whilst optical microscopes use visible light to create an image, uses electrons, and can view nanoparticles up to a resolution of 0.2 nm. Uranyl acetate is used as a negative stain, as it doesn't interact with protein, allowing for protein the be imaged against the stained electron dense background.

The method detailed by [108] is followed. A drop of AFt-PbS solution was deposited on the carbon coated copper grid. Any excess solution was removed with filter paper. Following this, a droplet of uranyl acetate solution was deposited on the grid for a few seconds, then the staining solution was removed with filter paper and the grid dried with N_2 gas. TEM images were acquired using JEOL1200EX and JEOL 2100F microscopes operating at 120 kV.

3.2.4 Photoluminescence spectroscopy

PL spectroscopy is a technique used to investigate the electronic structure of materials. It is a form of luminescence (light emission) that is initiated by photoexcitation (photons exciting electrons to a higher energy shell) after the direction of light onto a sample.

When light is directed onto a sample, the absorption of photons causes an electron to be transferred from a valance (highest occupied molecular orbital) to a conduction (lowest unoccupied molecular orbital) state. As a result, a photoexcited electron-hole pair is created. The recombination of photoexcited charges results in the emission of PL. The energy (or wavelength) of this emitted light is equal to the energy gap of the QDs. This data is beneficial because the energy gap in QDs depends on the size of the QD. Therefore, PL spectroscopy experiments can be used to determine the size of QDs.

3.3 Growth inhibitory studies

3.3.1 Cell culture

Cell lines used, MCF-7 and MDA-MB-468, were obtained from the American Type Culture Collection (ATCC) [109] [110]. MCF-7 cells are ER+, whilst MDA-MB-468 cells have a TNBC phenotype and express high levels of EGFR. The MCF-7 cells provided by ATCC are epithelial cells from a 69 year old female, who was diagnosed with adenocarcinoma. The MDA-MB-468 cells are epithelial cells from a 51 year old female who was also diagnosed with adenocarcinoma.

MycoAlert Mycoplasma Detection tests and Polymerase Chain Reaction (PCR) tests (performed by Haneen Abuzaid) were carried out to ensure the cells were mycoplasma free. Mycoplasma are self-replicating bacteria that cannot be seen under standard microscopes, and no not show any indication of being present such as cloudy media/ altered cell morphology. In cell culture, mycoplasma can compete for nutrients (and thus hinder cell growth), damage cell membranes and organelles, and cause mutations and chromosome changes. Therefore it is vital to ensure that cell lines are mycoplasma free.

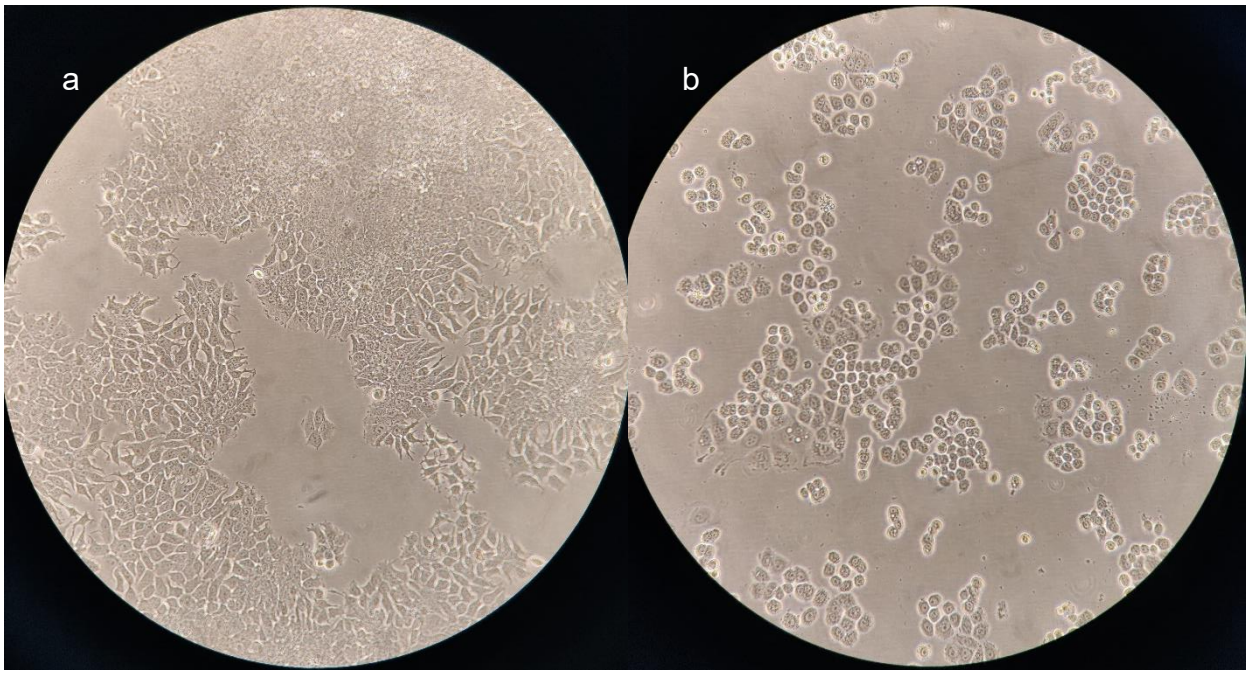

Figure 13. (a) MCF-7 cells. Passage 39, 8.2.21 (b) MDA-MB-468 cells. Passage 22 8.2.21. Images taken with a confocal microscope at 10x.

The cells were cultured in a solution of RPMI 1640 medium with 10% foetal bovine serum (FBS), and kept in an incubator at 37°C and 5% CO_2. When necessary 5 mL of 1% penicillin and streptomycin solution was included in culture medium to prevent bacterial growth in cell cultures. Cells were sub-cultivated twice weekly when they reached approximately 70-80% confluency, to maintain logarithmic growth rates. Cells were passaged up to 25 times to minimise phenotypic and genotypic drift.

3.3.2 MTT assay

MTT assays are a colourimetric assay, used to investigate the metabolic activity of a cell. They are indicative of cell viability, proliferation and cytotoxicity [111]. This assay is based on the reduction of a yellow tetrazolium salt to purple formazan crystals, by mitochondrial succinate dehydrogenase in metabolically active cells [111] (Figure 14). The darker the final solution, the greater the number of viable cells [111].

Disadvantages of this assay include the possibility that the number of mitochondria (and their metabolic rate) can vary in cells. This would impact the reaction that leads to formazan crystal formation.

Advantages of MTT assays include that they are rapid, reproducible and relatively inexpensive in comparison to other assays. Disadvantages of MTT assays can include the possibility that the number of mitochondria (and their metabolic rate) can vary in cells, thus impacting the reaction that leads to formazan crystal formation. Therefore, in cells with a low metabolism potentially 'bioactive' molecules may have a false negative result. In contrast, rapidly dividing cells exhibit high rates of formazan production.

Therefore, whilst this assay can provide useful information on cell cytotoxicity of drugs, it is important to conduct additional assays to corroborate observations of growth inhibition. In this case, we conducted clonogenic and cell count assays.

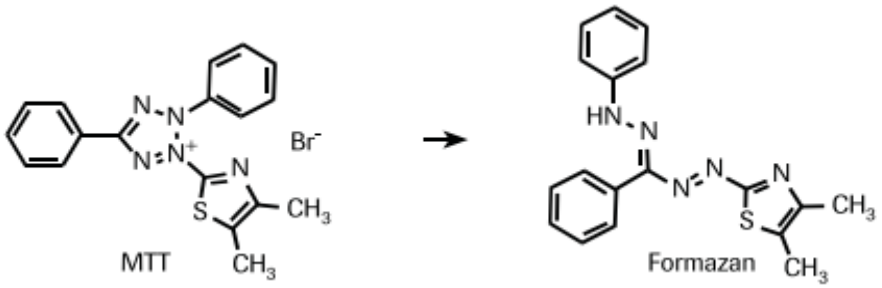

Figure 14. The conversion of MTT to formazan occurs *via* mitochondrial reductase. Figure reproduced from [111].

MTT assays were conducted in 96 well plates, with cells seeded at a density of 4000 cells per well and allowed 24h to adhere before introduction of test agent. The end column of each plate contained medium only as evaporation can occur from these wells, affecting cell growth and compound concentrations, eliciting a so-called `edge effect`. An extra plate was also prepared to carry out an MTT assay at the time of test agent addition (time zero, T0). On day 2, serial dilutions of test compounds were prepared at 10 times the required final concentration, and 20 µL was added to each well. At least three wells were used for each concentration. DMSO concentrations

were kept < 1%. Control cells were treated with medium alone or the appropriate vehicle control (DMSO or AFt). Following the required incubation time (72 h), 50 µL of 2 mg/mL MTT solution was added to each well (400 µL/mL final concentration). Cells were incubated for a further 3 h to allow formazan production. Formazan is utilised to indicate cell viability, as it indicates the amount of mitochondrial reductase present (Figure 14), and thus the number of viable cells. The aqueous medium was then aspirated and the formazan product solubilised in DMSO (150 µL/well). Absorbance of formazan at 570 nm (OD570) was read using an Anthos 2001 reader. Data were collected and analysed using Deltasoft 3 Software.

MTT assays were conducted for 5F 203, PbS QDs, AFt and DMSO. Estimated concentrations of test agents required to inhibit cells growth by 50% (GI_{50} values), 100% (total growth inhibition (TGI)), or kill 50% of cells initially exposed to test agent (LC_{50} values) were calculated where possible.

3.3.3 Clonogenic assay

Clonogenic assays were originally developed by Puck and Marcus in 1956 [112]. Clonogenic assays are an *in vitro* cell survival assay [113] used to determine the clonogenic capacity of a cell [114]. This can be defined as the ability of a single cell to survive a test agent challenge and proliferate to form a colony (a group of at least 50 cells) [113]. The ability of MCF-7 cells to form colonies after exposure to varying concentrations of 5F 203 were determined.

Clonogenic assays were conducted in 6 well plates, with cells seeded at a density of 250-350 cells per well, in 2 mL medium on day 1. On day two, the test agent was introduced and 24 h exposure was allowed. 3 wells were used per drug concentration. On day 3 the medium and test agent were aspirated from the wells, and wells were washed with medium. 3 mL medium was then added into the wells, plates were incubated for 7-10 days to allow colonies to grow. The time can vary, so it is important to monitor colony growth, and stop the assay when colonies in control wells contain > 50 cells. When colonies in control wells contain > 50 cells colonies are fixed, stained and counted. The medium was aspirated from the wells, and colonies washed in ice cold PBS (2x, 1 mL). The cells were fixed in 100% MeOH for 10 min (1 mL per well),

following which colonies were stained using 0.5 mL 0.05% methylene blue in 1:1 d.H_2O:MeOH, > 10 mins. Thereafter, the colonies were rinsed, air-dried and counted.

Clonogenic assays were conducted to determine the cytostatic and/or cytotoxic effects of 5F 203 on MCF-7 and MDA-MB-468 cell lines. A reduction in colony numbers indicates a cytotoxic response, whilst a reduction in colony size indicates a cytostatic response.

Estimated concentrations of test agents required to inhibit colony formation growth by 50% (IC_{50} values) were calculated. Plating efficiencies (*PE*) and survival fractions (*SF*) were calculated using Equations (2) and (3) [115].

$$PE = \frac{number\ of\ colonies\ formed}{number\ of\ cells\ seeded} 100\ \% \quad (2)$$

$$SF = \frac{number\ of\ colonies\ formed}{number\ of\ cells\ seeded(\frac{PE}{100})} \quad (3)$$

In addition to counting the number of colonies, colony area was analysed. Once stained, images were taken of the clonogenic plates on a white background. Using Image J, the area of the plates covered by cell colonies was counted.

3.3.4 Cell count assay

Cell count assays were performed to corroborate results obtained from MTT assays, to further validate cell viability and growth, and the cytostatic and /or cytotoxic nature of test agents under investigation. We measured the ability of MCF-7 and MDA-MB-468 cells to grow for 72 h after treatment with 5F 203.

Cell count assays were conducted in 6 well plates, with cells seeded at a concentration of 2 $x10^4$ in 2 mL medium. Cells were allowed 24 h to adhere, after which time, test agents were diluted to 3 times the required concentration in complete medium, and 1

mL added to each well. At least 3 wells were used for each test agent concentration for internal repeats. Following 72 h incubation, medium was aspirated, and 0.5 mL of trypsin was added to detach the cells from the plates. This was then neutralised with 0.5 mL medium. For MCF-7 cells, the medium was passed several times through a syringe and needle to prevent clumping and ensure the cells were in a single cell suspension. The cells were then counted using a haemocytometer. Cell count assays were conducted on MCF-7 and MDA-MB-468 cell lines, to assess the effect of 5F 203 on cellular growth. Internal repeats were conducted 3 times.

3.3.5 Statistical analysis

In this study, results were evaluated using Microsoft Excel version 2019. Representative figures are shown illustrating mean ± S.D. of a single trial where n = 3 internal replicates. Experiments were performed on ≥3 independent occasions. One and two-way ANOVA statistical analyses were applied to assess significant differences, which are defined as * ($P < 0.05$), ** ($P < 0.01$), *** ($P < 0.001$), **** ($P < 0.0001$).

Chapter 4: Results & Discussion

In the final theranostic nanoparticle, we aim to have 5F 203 and PbS QDs encapsulated inside the AFt protein cage. Here, the properties and cytotoxicity studies of individual 5F 203 and PbS on MCF-7 and MDA-MB-468 breast cancer cells are examined, to confirm their validity for the theranostic nanoparticle.

4.1. Encapsulation and characterisation

We explored two methods to encapsulate QDs and a therapeutic agent inside the AFt cage. These methods are reassembly and nanoreactor/diffusion (see Chapter 3.1.3). To encapsulate PbS QDs, the reassembly method detailed by Hennequin et al [107] was used. In this approach, preformed PbS QDs are added to dissembled AFt, following which the AFt is reassembled by increasing the pH of the solution.

To encapsulate 5F 203 inside AFt, the nanoreactor method detailed by Breen [80] was used (Figure 15). In this method 5F 203 molecules enter the AFt cavity through the hydrophobic and hydrophilic channels, due to passive diffusion (see Chapter 3.1.4). This method was found to be the most effective as its was able to encapsulate the most 5F 203 molecules per AFt [80]. In the research reported in [80], 100 5F 203 molecules were encapsulated per AFt molecule, totalling to 29.16 μM.

During the analysis of encapsulation, problems with the reassembly method arose, as it was difficult to reform the AFt at the correct size [80]. In addition, AFt precipitation occurred during pH changes [80]. These problems were solved by utilising the nanoreactor method, thus meaning that the nanoreactor method for encapsulation was the most efficient.

The combination of these methods would allow encapsulation of drug molecules into the protein containing imaging agents, as PbS QDs would be entrapped first with the disassembly and reassembly of AFt. Then following this, drug molecules such as 5F 203 could be encapsulated *via* passive diffusion (nanoreactor method), allowing the encapsulation of both molecules simultaneously (Figure 15).

To analyse the encapsulated 5F 203 and PbS QDs, TEM, DLS and PL studies were conducted. The amount of encapsulated 5F 203 was determined *via* UV-vis experiments and Bradford assays.

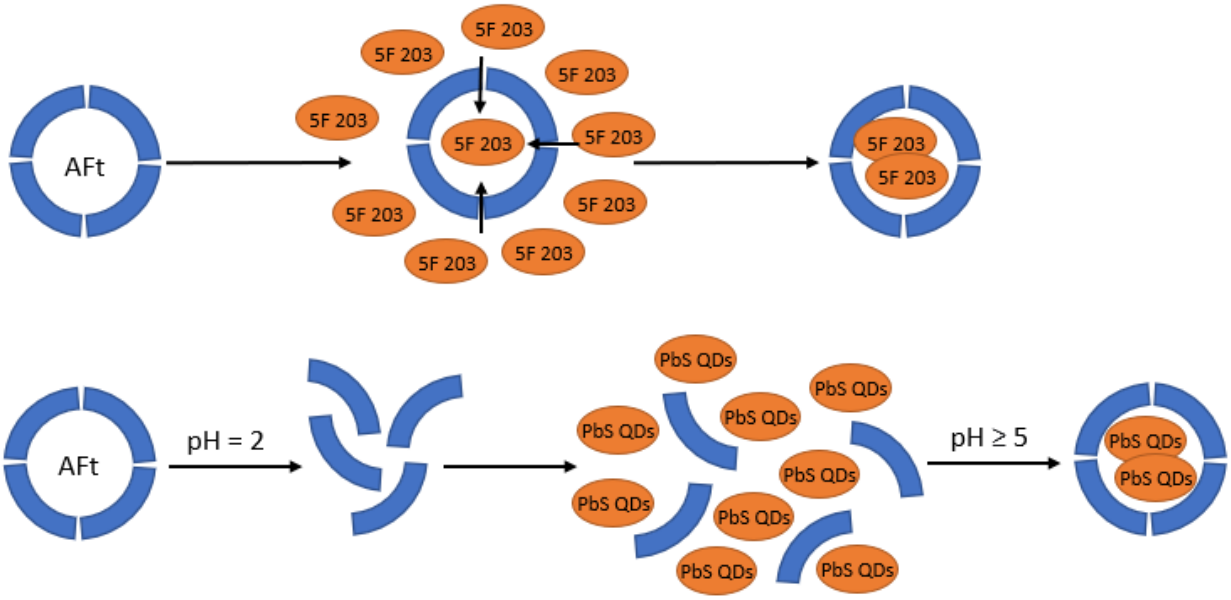

Figure 15: AFt encapsulation routes. Nanoreactor (top) and reassembly (bottom) encapsulation. Figure recreated from [80].

4.1.1 Transmission electron microscopy images of quantum dots

TEM experiments were conducted to analyse the size of the encapsulated AFt-PbS nanoparticle and to confirm the presence of QDs in the final compound. The first TEM experiment conducted confirmed the presence of PbS QDs (Figure 16). TEM images revealed the presence of electron dense particles (the spherical shapes in the image) corresponding to PbS QDs. We note, that in this image, the QDs are assembled into macroscopic rod-like structures. The nature of this assembly is not yet understood and is likely driven by the presence of sodium acetate from the buffer solution used [116]. However, the TEM imaging is unable to reveal the AFt protein shells, as they are not electron dense. Therefore the AFt-PbS QDs were deposited onto a carbon grid and stained with heavy metal salt, uranyl acetate. The salt of uranyl acetate covers the empty parts of the grid, but does not interact with the protein, hence protein can be imaged against the stained electron dense background (Figure 17). At the areas with

higher density of the sample, the protein capsules are assembled into hexagonal packaging. This packing has been reported before in research by Takeda *et al* [117], and is driven by the presence of cadmium sulphate [117].

Using ImageJ, we were able to determine that the length of the PbS nanoparticles shown in Figure 16 was 4.1 ± 1.6 nm (*n = 30*). These results corroborate with previous research by Turyanska *et al* [102], that found the size of PbS nanoparticles to have an average diameter of 5 ± 2 nm. The length of the AFt-PbS nanoparticles shown in Figure 17 was 12 ± 1 nm (*n=30*). This corroborates with research by Turyanska *et al* [90] [118] that shows the average diameter of AFt nanoparticles is 12 ± 1 nm, as expected for AFt. We can therefore conclude that the encapsulation of PbS QDs *via* reassembly does not affect the final size of AFt.

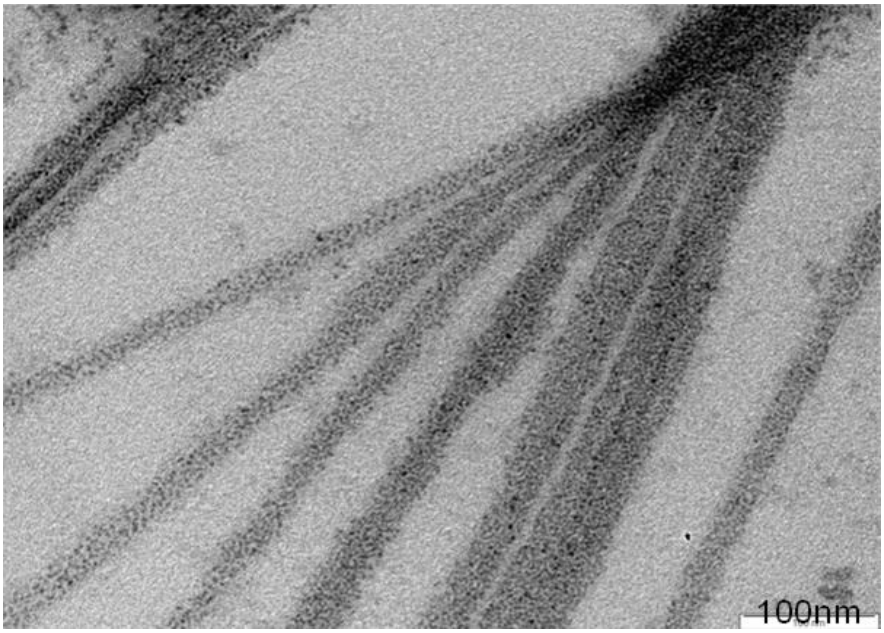

Figure 16. TEM image of PbS nanoparticles encapsulated in AFt *via* the nanoreactor route. Figure provided by Dr Turyanska.

Energy dispersive X-ray spectroscopy was also used to confirm the presence of the PbS QDs in the stained AFt-PbS samples. This is an analytical technique used for the elemental analysis of a sample. Figure 17 shows characteristic peaks for Cu, Pb and S. The Cu peaks are present due to the carbon coated copper grid where the sample is deposited, and the Pb and S peaks confirm the presence of PbS QDs. Therefore,

based on combination of unstained and stained TEM images and the EDX we estimated the size of the QDs and confirmed presence of intact AFt shells containing QDs.

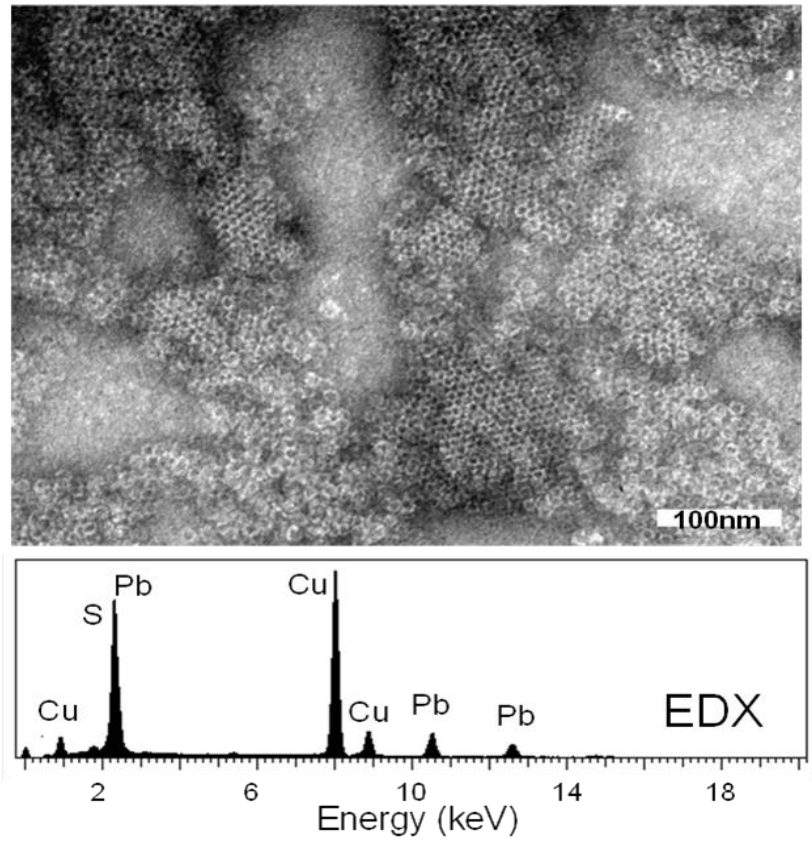

Figure 17. A TEM image of AFt-PbS produced *via* the nanoreactor route, negatively stained with uranyl acetate showing AFt protein cages, and EDX spectrum. Figure provided by Dr Turyanska.

4.1.2 Dynamic light scattering

DLS experiments were used to determine the size and distribution of the particles. In this experiment, stock AFt (AFt before reassembly) was used as a control sample. We assessed the size of the protein capsule before and after pH driven reassembly to see if the mean diameter of AFt changed.

In DLS experiments, the size and distribution of the nanoparticles were measured as a number distribution, and a volume distribution, which relates to the volume filled by particles with different sizes (Section 3.2.1). The results of the DLS measurements are

shown in Figures 18 and 19, and show the mean hydrophobic diameters expressed as number and volume percentages.

The hydrophobic diameters of the stock and reassembled AFt are 11.9 ± 1.4 nm and 12.9 ± 1.3 nm *(n=3)* respectively (Figure 18). The p value was calculated to be 0.623, so we can conclude that there is no significant difference in the mean number hydrophobic diameters. We can therefore conclude that AFt forms into the same shape when dissembled and reassembled *via* pH. There are some changes between the repeats, where we observe particle size decreasing with each repeat.

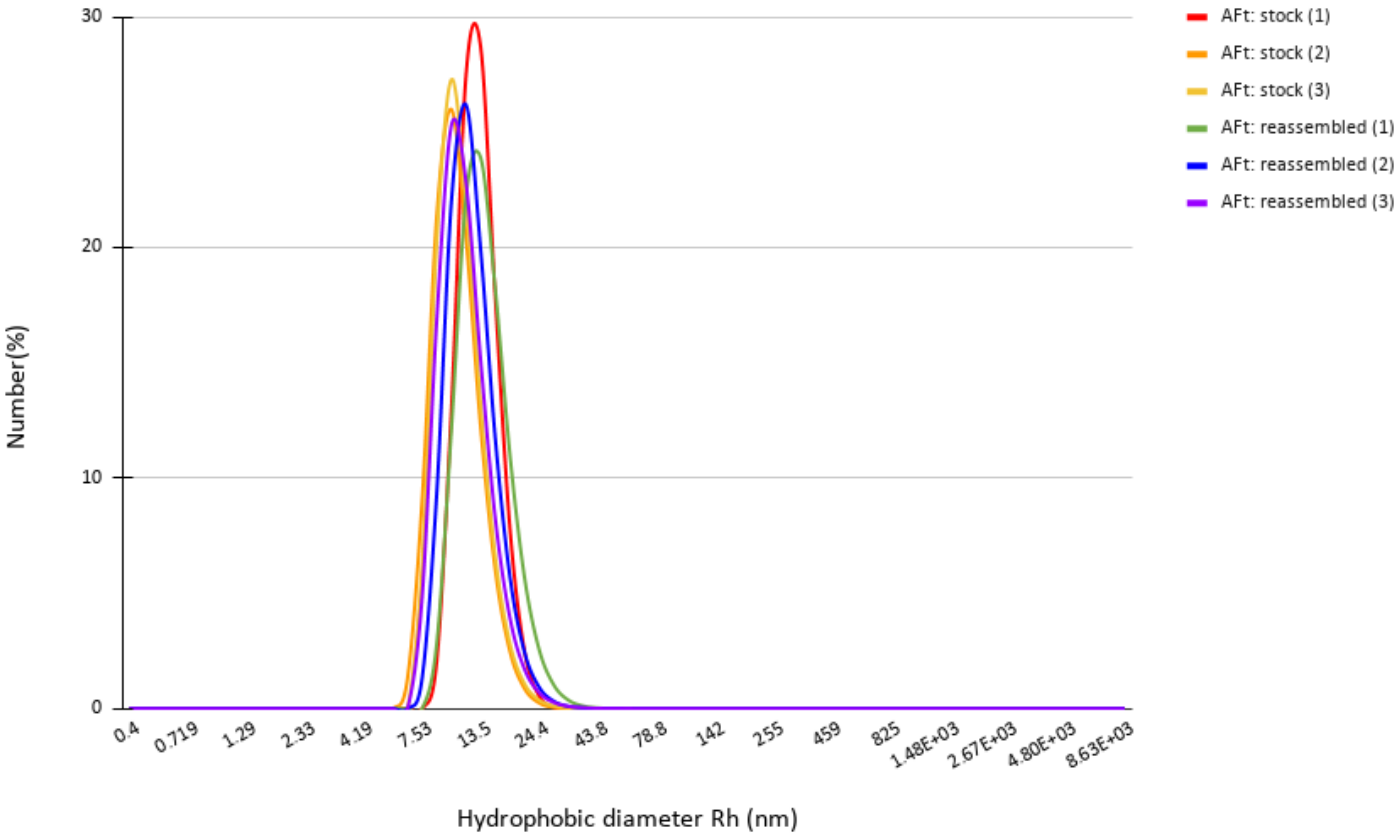

Figure 18: The mean number hydrodynamic diameter (nm) of stock AFt and reassembled AFt. Temperature was maintained at 25 °C, and data points are mean +/- S.D., *n* = 3. Experiments performed by Haneen Abuzaid.

Using DLS analysis by volume, hydrophobic diameters of the stock and reassembled AFt are found to be 20.2 ± 1.2 nm and 19.1 ± 1.3 nm (*n=3)* respectively (Figure 19).

The p value was calculated to be 0.502, hence there is no significant difference in the hydrodynamic diameters. This further confirms that pH driven assembly of AFt allows AFt to reform into the same shape as the stock AFt. The hydrophobic diameters estimated from analysis by volume are greater than those estimated from analysis by number, which could be attributed to presence of AFt dimers in the solution. AFt's ability to dimerise has been proved previously by native-PAGE experiments [119], and it is for this reason the mean volume diameter is greater than 12 nm.

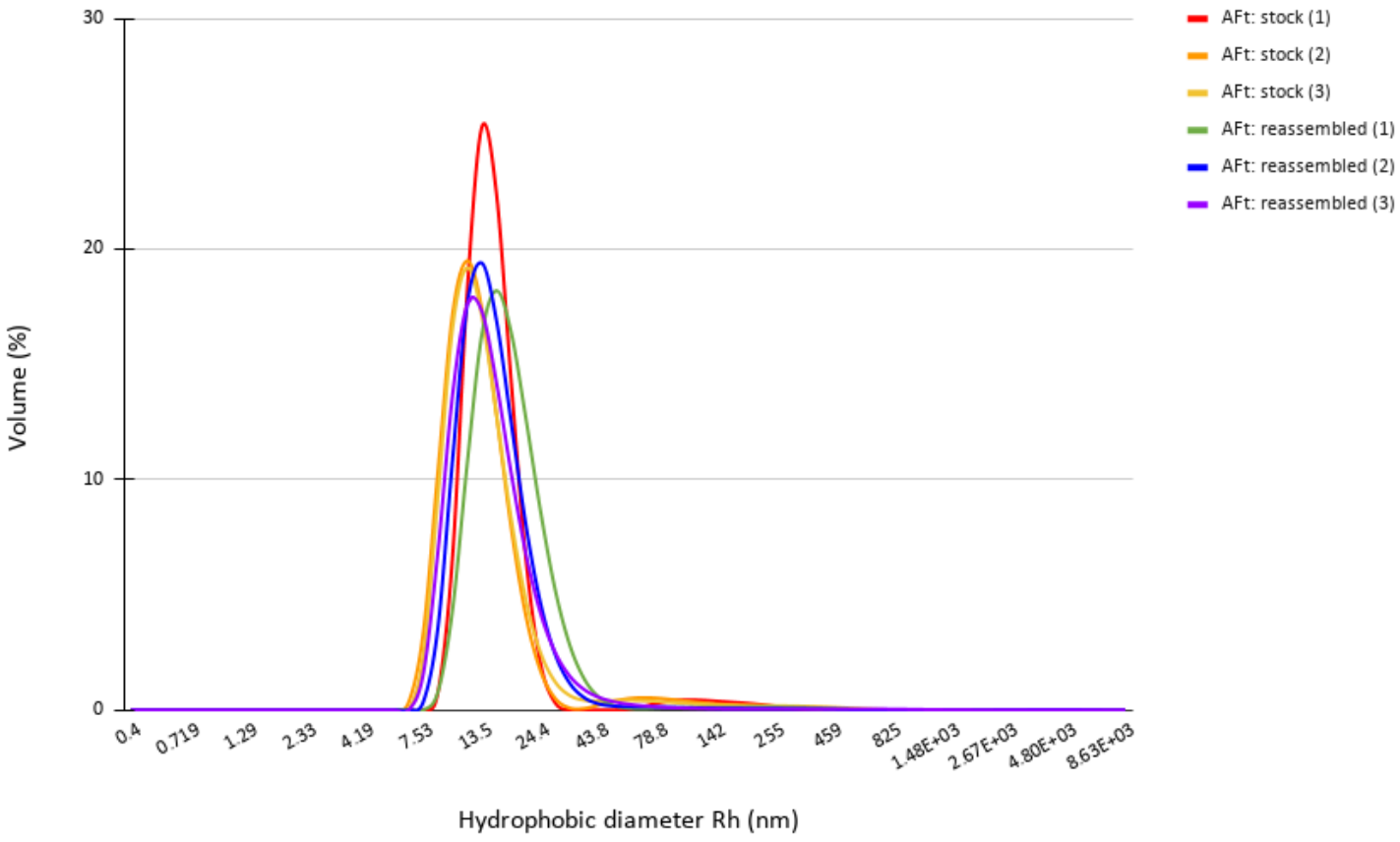

Figure 19: The mean volume hydrodynamic diameter (nm) of stock AFt and reassembled AFt. Temperature was maintained at 25 °C, and data points are mean +/- S.D., *n* = 3. Experiments performed by Haneen Abuzaid.

Previous research by Zamberlan *et al* [105] had measured the average hydrodynamic diameter of reassembly AFt encapsulated PbS QDs to be 11 ± 1 nm. This data supports the DLS data obtained here, and it is therefore possible to conclude that reassembly AFt encapsulation of PbS QDs does not change the final shape.

4.1.3 Photoluminescence spectroscopy data

PL spectroscopy was used to measure the energy of the PL peak, which is related to the size of QDs, as explained in Chapter 3.2.4. We utilised PL spectroscopy to analyse PbS QDs and PbS QDs encapsulated in AFt *via* reassembly route. These investigations are also important as an indication of the potential of QDs for use as imaging agents.

The PbS QD sample has PL emission with a peak centred at 1141 nm, and a full width at half maximum (FWHM) of ~ 150 nm (Figure 20a). After the encapsulation (Figure 20b), we observed a small shift of the PL peak of the AFt-PbS QDs to 1162 nm, with a FWHM of 152 nm.

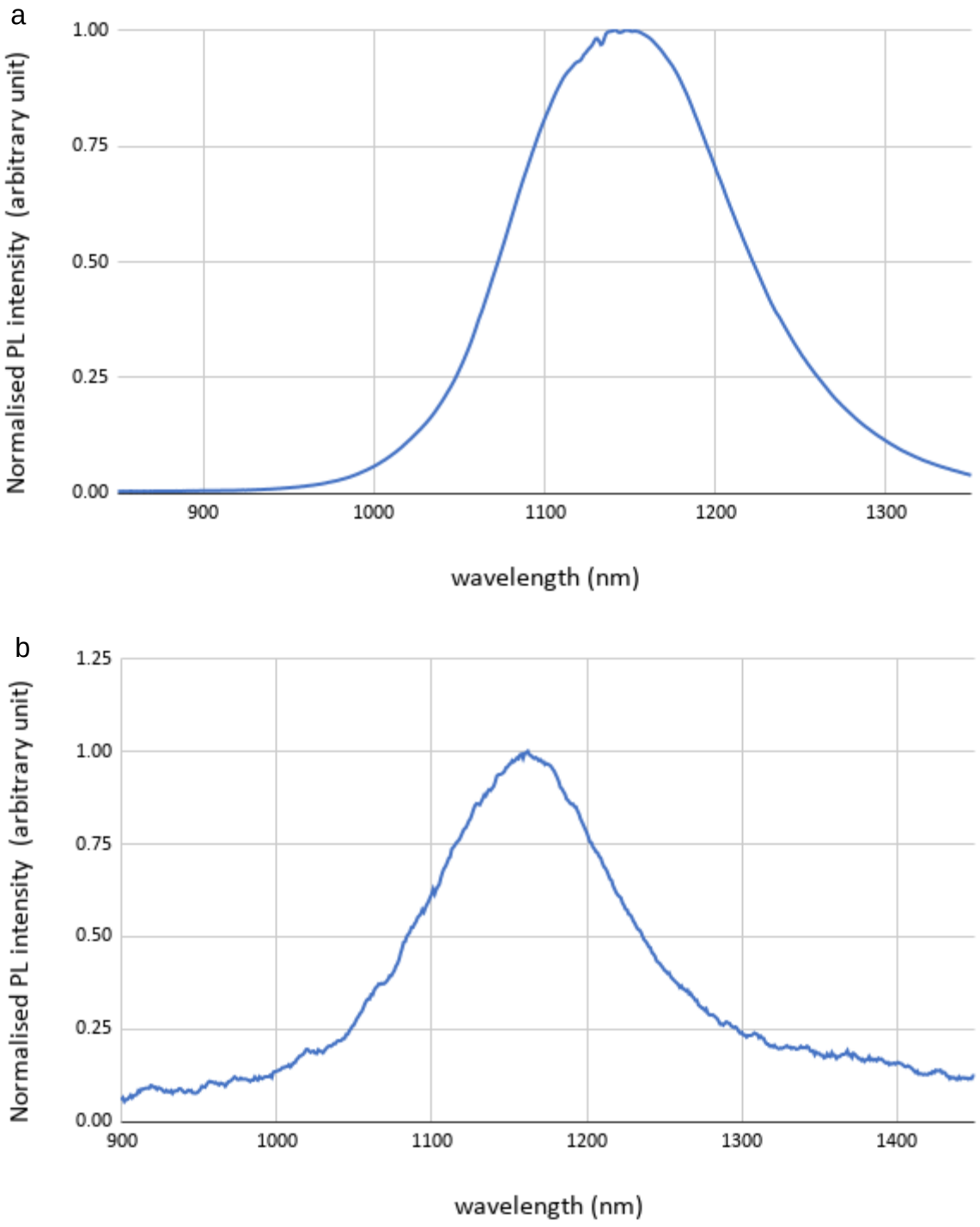

Figure 20. Room temperature PL spectra of solutions of (a) PbS QD (Pb:S =1:0.3), and (b) AFt-PbS QD (Pb:S =1:0.3) prepared using reassembly method.

As shown in Figure 20, there is a 21 nm difference between the PL peak position of PbS QDs and AFt-PbS QDs, whilst the FWHM values remain the same. The shift of the PL peak after encapsulating could be indicative of the presence of larger QDs in

the AFt-PbS , compared to the PbS QDs, as larger QDs emit at longer wavelengths [107]. The linewidth remained unchanged, hence indicating that the encapsulating process has not affected the size distribution of the QDs.

In summary, the PL data confirms the potential of encapsulated QDs for imaging. As the PL intensity of the PbS QDs, and AFt encapsulated PbS QDs have no significant difference, this indicates that encapsulated QDs still have the same imaging benefits as non-encapsulated QDs. This is useful as non-encapsulated PbS QDs are cytotoxic to healthy cells, but their encapsulation in AFt would allow for the targeting of cancer cells (Section 1.7) (whilst providing the imaging benefits).

Results reported by Zamberlan *et al* [105] showed that reassembly encapsulated PbS QDs has PL emissions tuneable in the NIR range from 920 nm to 1220 nm. Therefore, the results shown in Figure 20 corroborate with this. In addition, PL emissions at this wavelength are beneficial for imaging, as they benefit from low absorption by biological tissues and lower light scattering, resulting in deeper tissue penetration of the emitted light (Section 1.8).

4.2 Growth inhibitory studies

MTT assays were conducted to examine the effects of 5F 203, AFt, PbS and DMSO on growth of the breast cancer cell lines. Both MCF-7 and MDA-MB-468 were selected as they are both breast cancer cell lines that have been shown to express inducible *cyp1a1*. This gene expression is important as the CYP1A1 protein is responsible for benzothiazole metabolism, resulting in cell death (Section 1.5.1).

4.2.1 *In vitro* activity of apoferritin

MTT assays were conducted with AFt, to confirm that it acts as a non-toxic drug delivery vehicle. The results of the MTT assays in the MCF-7 cell line showed that AFt had negligible effect on the cell viability (measured as mitochondrial activity) at concentrations ≤ 1464.93 nM (Figure 21). Similarly, the results of the MTT assays in the MDA-MB-468 cell line showed that AFt had no effect on cell viability (mitochondrial activity) at concentrations ≤ 1464.93 nM (Figure 22).

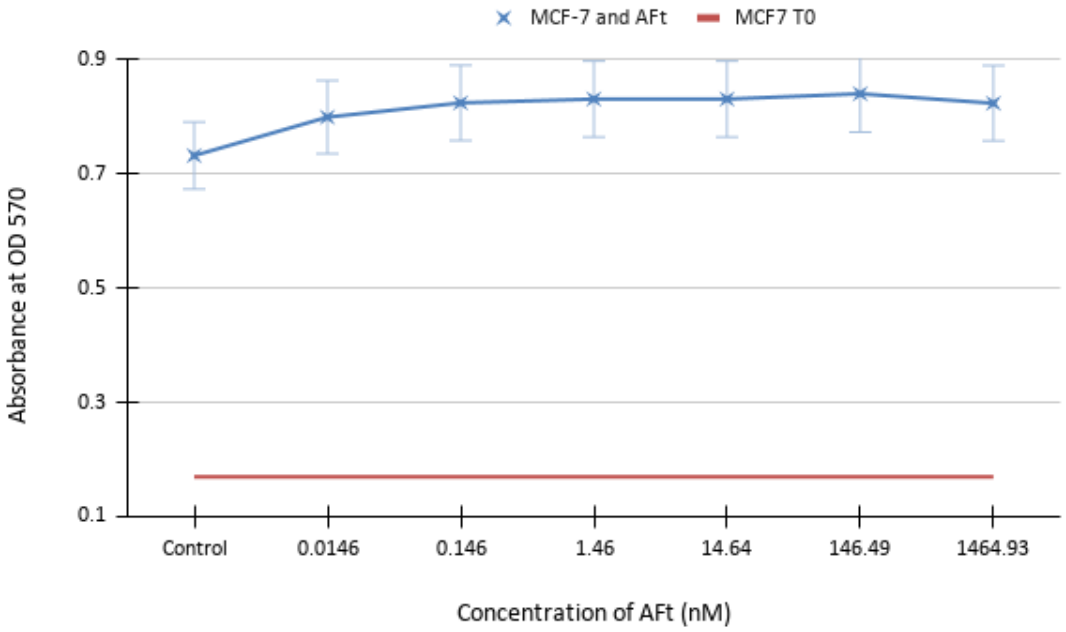

Figure 21: MTT assay dose response curves showing the effects of AFt on MCF-7 cells. MCF-7 cells were seeded at a density of 4000 cells per well, in 96 well plates and incubated overnight. Cells were then treated with AFt at 0.0146, 0.146, 1.46, 14.64, 146.49, 1464.93 nM for 72h. Data points represent mean +/- S.D., *n=6* from 1 trial; 3 independent trials were conducted.

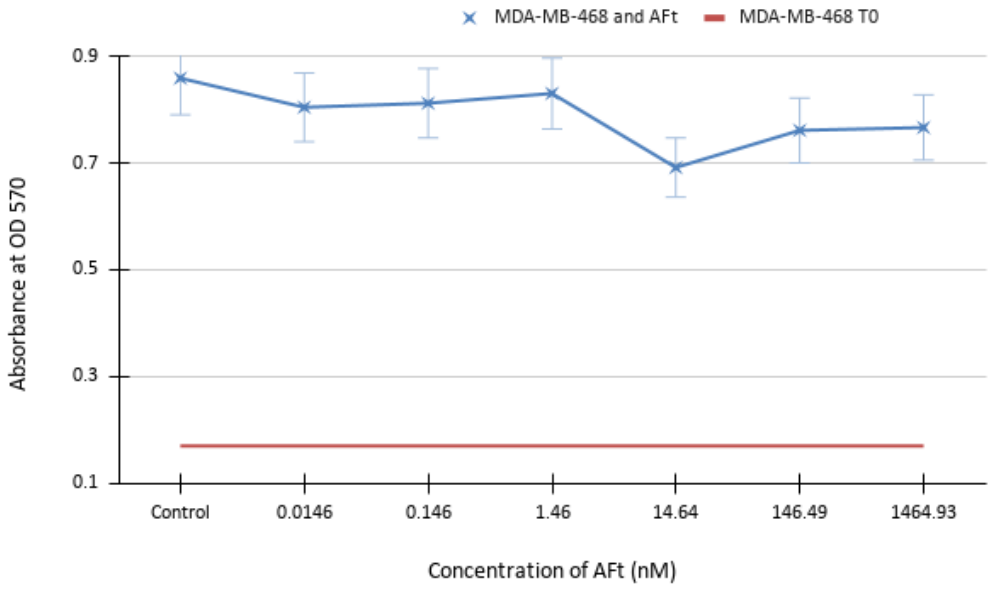

Figure 22: MTT assay dose response curves showing the effects of AFt on MDA-MB-468 cells. MDA-MB-468 cells were seeded at a density of 4000 cells per well, in 96 well plates and incubated overnight. Cells were then treated with AFt at 0.0146, 0.146, 1.46, 14.64, 146.49, 1464.93 nM for 72h. Data points represent mean +/- S.D., *n=6* from 1 trial; 3 independent trials were conducted.

These results are supported by previous research into the effect of AFt on cells by Breen *et al* [80]. MTT and clonogenic assays conducted by Breen found AFt had no effect on MCF-7 cells and HCT-116 cells, up to concentrations of 2262.25 nM.

4.2.2 *In vitro* activity of DMSO

In addition to investigating AFt, DMSO was also investigated to confirm that it acts as a non-toxic solvent for 5F 203, and does not affect cell proliferation at concentrations equivalent to those present in 5F 23 dilutions. The results of the MTT assays in the MCF-7 cell line shows that DMSO had a negligible effect on cell proliferation ≤ 0.5% (Figure 23). This is supported by research by Breen [80] that found that DMSO had no effects on cell viability of MCF-7, MDA-MB-468, HCT116 and MCR-5 cells up to concentrations ≤ 0.5%. We can therefore conclude that the DMSO did not affect cell growth or viability, and thus results from MTT assays were due to the effect of 5F 203 alone.

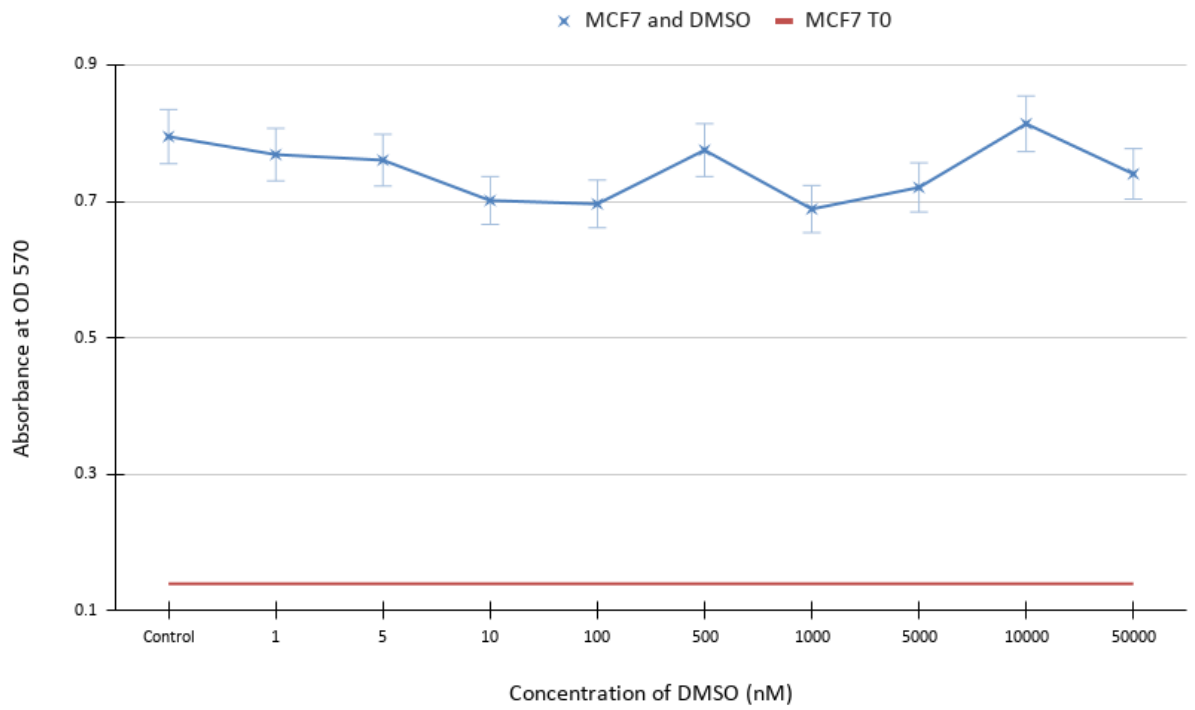

Figure 23: MTT assay dose response curves showing the effects of DMSO on MCF-7 cells. MCF-7 cells were seeded at a density of 4000 cells per well, in 96 well plates and incubated overnight. Cells were then treated with DMSO at concentrations of 0.00001, 0.00005, 0.0001, 0.001, 0.01, 0.05, 0.1, and 0.5% for 72h. Following this, plates were read using a Wallac envision plate reader. Data points are mean +/- S.D., *n* = 6

4.2.3 *In vitro* activity of 5F 203

The MTT dose response curves for 5F 203 (Figure 24) shows that the MCF-7 cells are responsive to 5F 203 treatment with a mean GI_{50} value of 7.4 ± 0.95 nM. The dose response curve does not drop below the time zero line (T0), suggesting that 5F 203 has a net cytostatic effect on MCF-7 cells [3]. The MTT dose response curves for 5F 203 (Figure 25) shows that the MDA-MB-468 cells are responsive to 5F 203 treatment with a mean GI_{50} value of 6.4 ± 0.5 nM. The dose response curve falls below the time zero line (T0), suggesting that 5F 203 exerts a net cytotoxic effect on MDA-MB-468 cells at concentrations ≥ 50 nM.

These findings suggest that MDA-MB-468 cells are more sensitive to 5F 203 treatment than MCF-7 cells. This could possibly be due to a greater presence of AhR receptors, but further research would be required to confirm this. The cytotoxicity shown by these results can be explained by the mechanism of action of 5F 203. 5F 203 works by binding to the AhR receptor, resulting in the translocation of the ligand-bound receptor complex into the cell nucleus. Ensuing dimerisation with the AhR nuclear transporter (ARNT) and binding to the xenobiotic response element (XRE) of genes in the AhR battery, including *cyp1a1* results in the activation of *cyp1a1* gene transcription. The CYP1A1 enzyme produced metabolises 5F 203 into reactive intermediates (electrophilic species) that attack the cells` DNA at nucleophilic sites causing adduct formation, ultimately resulting in cell death [120].

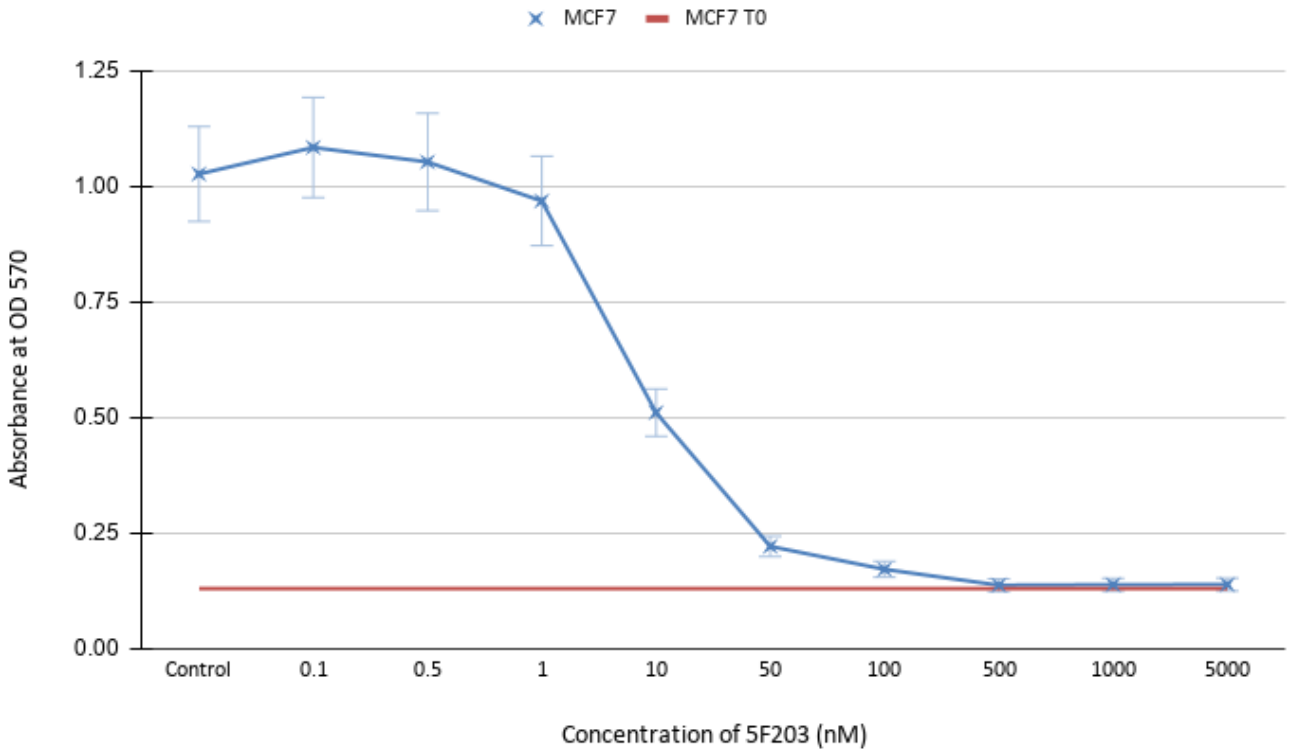

Figure 24: A representative MTT assay dose response curves showing the effects of 5F 203 on MCF-7 cells. MCF-7 cells were seeded at a density of 4000 cells per well in 96 well plates and incubated overnight. Cells were then treated with 5F 203 at 100 pM, 500 pM, 1 nM, 10 nM, 50 nM, 100 nM, 1 µM and 5 µM for 72h. Data points represent mean +/- S.D., *n*=6 from 1 trial; 3 independent trials were conducted.

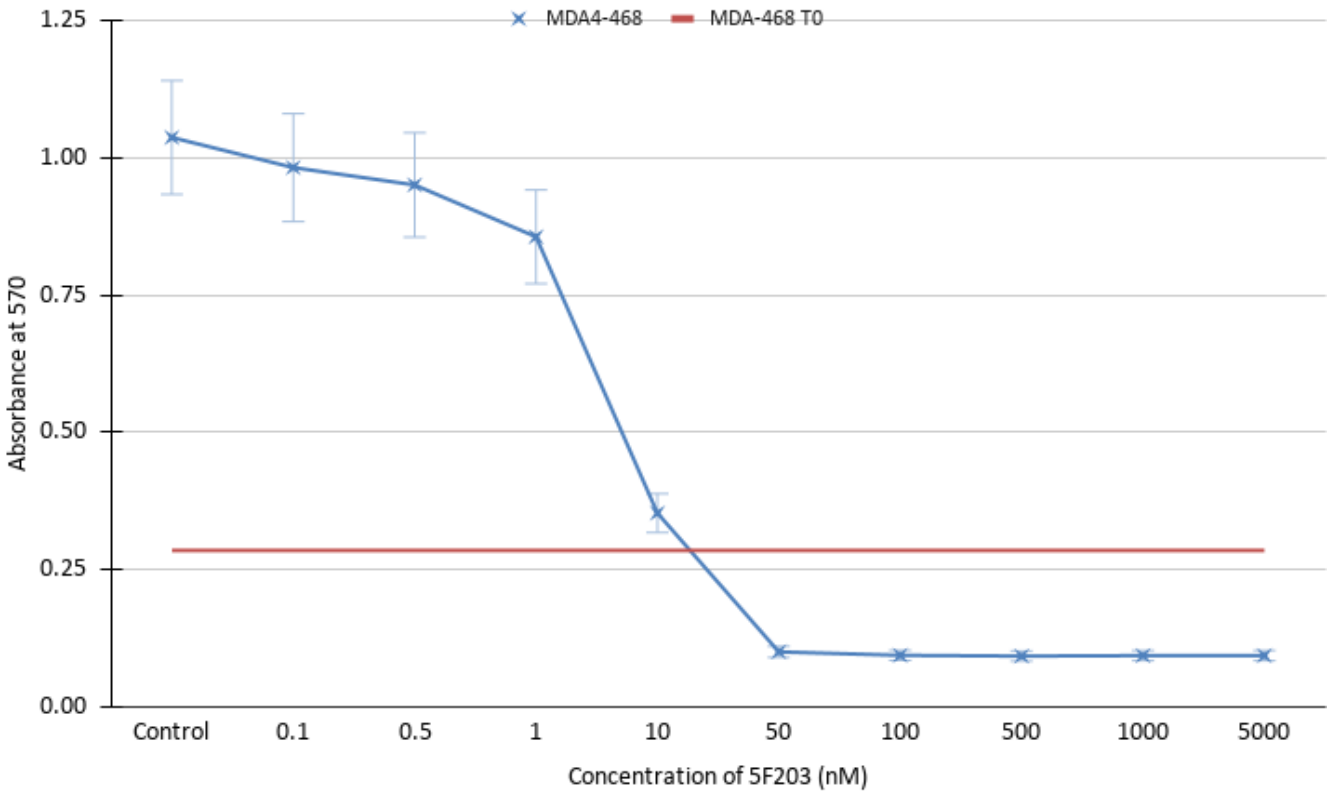

Figure 25: A representative MTT assay dose response curves showing the effects of 5F 203 on MDA-MB-468 cells. MDA-MB-468 cells were seeded at a density of 4000 cells per well, in 96 well plates and incubated overnight. Cells were then treated with 5F 203 at 100 pM, 500 pM, 1 nM, 10 nM, 50 nM, 100 nM, 1 µM and 5 µM for 72h. Data points are mean +/- S.D., *n*=6 in single representative experiment; 3 independent trials were conducted.

In addition to my data, data in the literature also show the effects of 5F 203 on cells expressing CYP1A1. For example, research by Breen found that MCF-7 cells had a GI_{50} value of 4.9 ± 0.6 nM, whilst HCT-116 cells showed no response to treatment [80]. The lack of response by HCT-116 cells was because they express neither constitutive not inducible CYP1A1 enzyme [80]. In addition, research by Yang *et al* concluded that 5F 203 had a IC_{50} value of 3.45 ± 1.05 nM in MCF-7 cells [121].

4.2.4 *In vitro* activity of lead sulphide quantum dots

The MTT dose response curves for PbS QDs (Figure 26) shows that the MCF-7 cells are responsive to PbS QD treatment with a mean GI_{50} value of 3.92 ± 1.33 µg/mL. The dose response curve drops below the time zero line (T0), suggesting that PbS QDs have a cytotoxic effect on MCF-7 cells at concentrations ≥ 3.8 µg/mL.

The GI_{50} values obtained in my experiments are summarised in Table 1 below and demonstrate the concentration of test agent required to cause a 50% reduction in the proliferation of cancer cells.

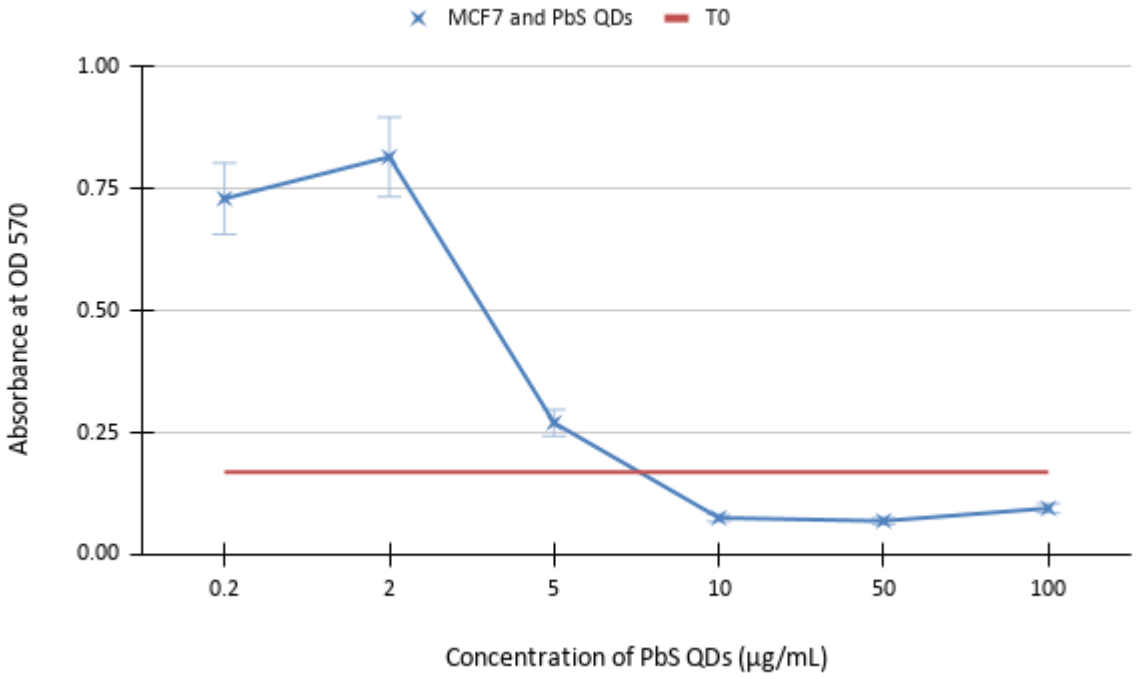

Figure 26: A representative MTT assay dose response curves showing the effects of PbS on MCF-7 cells. MCF-7 cells were seeded at a density of 4000 cells per well, in 96 well plates and incubated overnight. Cells were then treated with PbS at 0.2, 2, 5, 10, 50, and 100 µg/mL for 72h. Data points are mean +/- S.D., *n*=6.

Table 1: Summary of GI_{50} values calculated from 4 (3 for MCF-7) independent MTT assays. Cells were exposed to test agents for 72 h. Mean ± S.E.M. with *n = 6.*

	Cell line and compound		
	MCF-7 5F 203 (nM)	**MDA-MB-468 5F 203 (nM)**	**MCF-7 PbS (µg/mL)**
GI_{50} values	6.11	6.51	2.99
	9.25	7.55	4.85
	6.90	5.15	
		6.51	
Mean GI_{50} value (± S.E.M.)	7.42 ± 0.95	6.43 ± 0.50	3.92 ± 1.33

Previous research has found that the cell cycle of non-tumourigenic cells is not altered by exposure to AFt-PbS up to concentrations of 1 mg/mL [102], indicating that PbS QDs negligibly impact non tumourigenic cells at concentrations < 1 mg/mL. However, human derived MCF-7 carcinoma cells were altered at concentrations of PbS QDs > 0.2 mg/mL [102], and colorectal cancer cell lines revealed a GI_{50} of 70 ug/mL [103] (when challenged with PbS QDs). These data therefore corroborate my results, showing that PbS QDs have a cytotoxic effect on cancer cells.

In summary, MTT assays were conducted in MCF-7 and MDA-MB-468 breast cancer cell lines, to determine the effects of 5F 203, AFt, PbS and DMSO on cell growth and viability. The results of the MTT assays showed that 5F 203 had growth inhibitory and cytotoxic properties, with high potency at low nM concentrations in MCF-7 and MDA-MB-468 cell lines. AFt and DMSO have been shown to be non-toxic at the concentrations tested and have no effect on MCF-7 cells` proliferation, meaning that all effects exhibited were due to 5F 203 exposure. In the future, it would be beneficial to test these agents against MDA-MB-468 cells also. The results showed that PbS QDs exerted cytotoxic effects against MCF-7 cells. In the future it would be beneficial to test the growth inhibitory and cytotoxic effects of PbS QDS against MDA-MB-468 cells also.

4.3 Cell count assays

In addition to conducting MTT assays, cell count assays were conducted to analyse the effect of 5F 203 on MCF-7 and MDA-MB-468 cells. Similarly to MTT assays, cell count assays are conducted over 72 hours.

The assay results show that the MCF-7 cells are responsive to 5F 203 treatment with a mean GI_{50} value of 26.32 nM. In addition, we can conclude that the MDA-MB-468 cells are also responsive to 5F 203 treatment, with a mean GI_{50} value of 27.21 nM. The GI_{50} values for individual experiments are summarised in Table 2 and demonstrate the concentration of test agent required to cause a 50% reduction in the growth of breast cancer cells.

These findings corroborate the MTT results obtained, demonstrating that ER+ MCF-7 and TNBC MDA-MB-468 cell growth is potently inhibited by nM 5F 203 concentrations. Cell count assays are useful to rule out the possibility of a false positive result (due the mitochondrial inhibition) from the MTT assay.

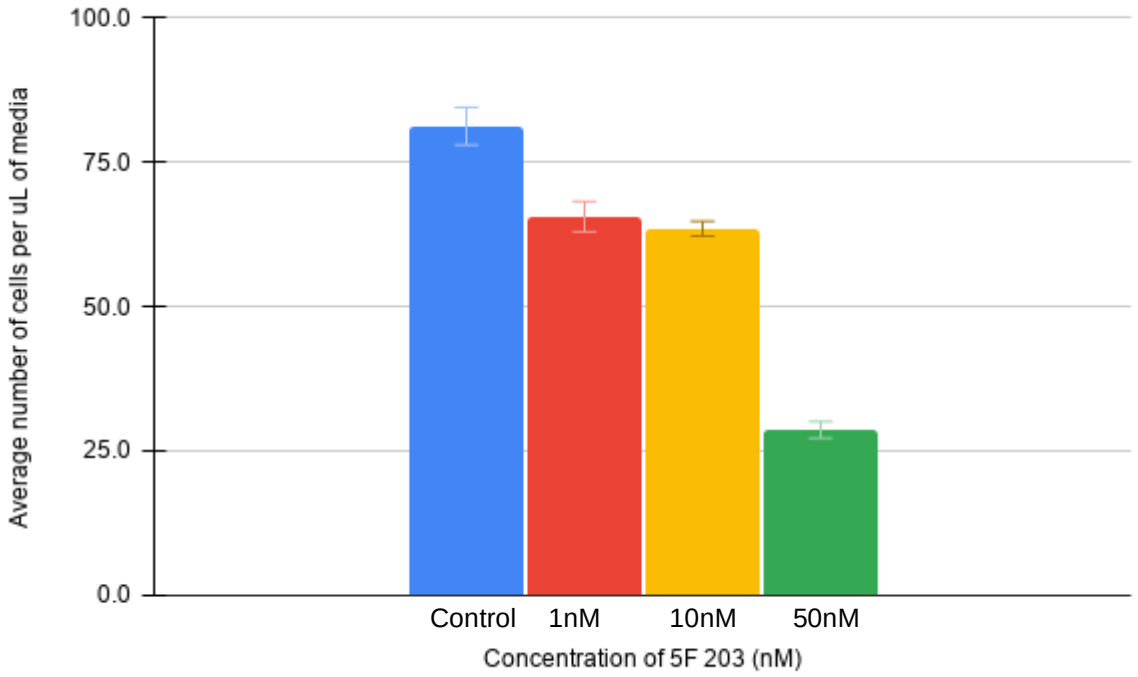

Figure 27: Cell count assay showing the effects of 5F 203 on MCF-7 cell growth. MCF-7 cells were seeded at a density of 20,000 cells per well, in 6 well plates and incubated overnight before treatment with 5F 203 at 1 nM, 10 nM and 50 nM for 24h. Cells were left for 72h to grow, then harvested and counted with a haemocytometer. Data points are mean +/- S.D. from one representative graph where internal repeats *n*=6. The experiment was repeated on 2 independent occasions.

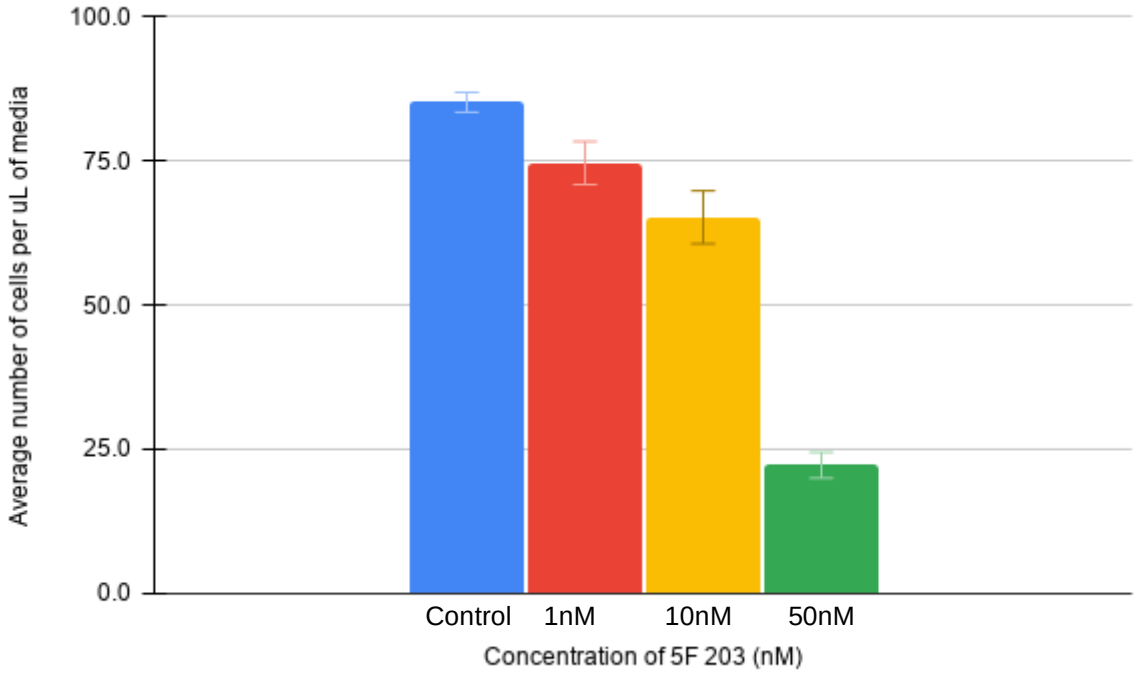

Figure 28: Cell count assay showing the effects of 5F 203 on MDA-MB-468 cell growth. MDA-MB-468 cells were seeded at a density of 20,000 cells per well, in 6 well plates and incubated overnight before treatment with 5F 203 at 1 nM, 10 nM and 50 nM for 24h. Cells were left for 72h to grow, then harvested and counted with a haemocytometer. Data points are mean +/- S.D. from one representative graph where internal repeats *n*=6. The experiment was repeated on 3 independent occasions.

Table 2: Summary of GI_{50} values taken from 3 independent cell count (72 h exposure to 5F 203) assays. Mean ± S.E.M. *with n = 6.*

	Cell line and compound	
	MCF-7 5F 203 (nM)	**MDA-MB-468 5F 203 (nM)**
GI_{50} values	23.72	33.53
	28.91	22.68
		25.41
Mean GI_{50} value (± S.E.M.)	26.32 ± 1.83	27.21 ± 3.26

4.4 Cell survival assays

By conducting MTT and cell count assays, we can conclude that 5F 203 potently inhibits growth of the 2 mammary carcinoma cell lines tested. In order to evaluate whether 5F 203 exerts a cytotoxic response, clonogenic assays were performed. As explained in Section 3.4.2, clonogenic cell assays are a type of *in vitro* cell survival assay [113]. We are testing ability of single cell to survive brief (24 h) challenge and produce progeny colony. A reduction in colony number indicates a cytotoxic response, whereas a reduction in colony size (with a change in colony numbers) would indicate a cytostatic response.

The MCF-7 cells showed a consistent decrease in the number of colonies formed as the concentration of 5F 203 was increased (Figure 29). The mean IC_{50} value was calculated to be 10.84 nM (Table 2), indicating that 10.84 nM was required to inhibit colony formation (in number) by 50%. In addition, the MCF-7 cells also showed a constant decrease in the area (size, therefore cell numbers within colonies) of the colonies formed with an increase in concentration of 5F 203 (Figure 30). The mean IC_{50} value of four independent repeats (3 experiments conducted by myself, 1 set of data provided) for MCF-7 cells was 7.17 nM (Table 2), indicating that 7.17 nM 5F 203 is required to observe 50% inhibition of the area of the cell colonies. The reduction in colony number shown in Figure 30 indicates that 5F 203 is cytotoxic towards MCF-7 cells. We can conclude that the 2 values show consistency, and that nM values of 5F 203 are able to inhibit total colony area and colony numbers.

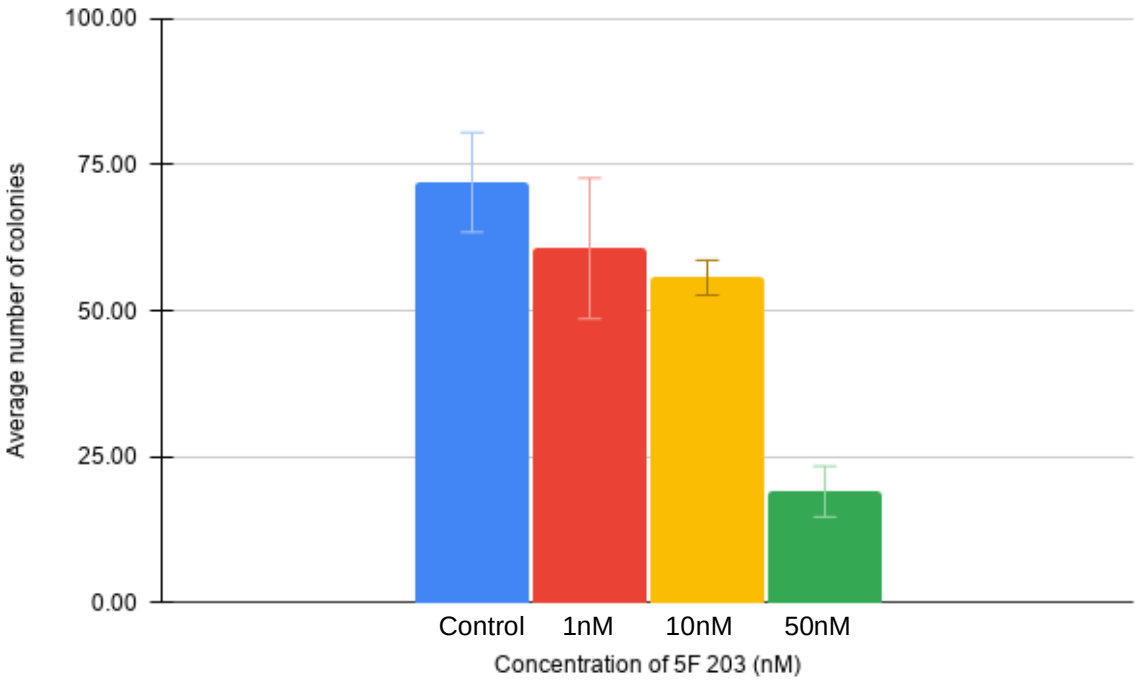

Figure 29: Clonogenic cell survival assay showing the effects of 5F 203 on colony formation with respect to the number of colonies. MCF-7 cells were seeded at a density of 250 cells per well, in 6 well plates and incubated overnight before treatment with 5F 203 at 1 nM, 10 nM and 50 nM for 24h. Cells were left for 6-8 days to form colonies, and then read when there were more than 50 cells in the control wells. Data points show mean and S.D. from one representative graph where internal repeats $n = 4$. Clonogenic plates provided by Dr Bradshaw for analysis.

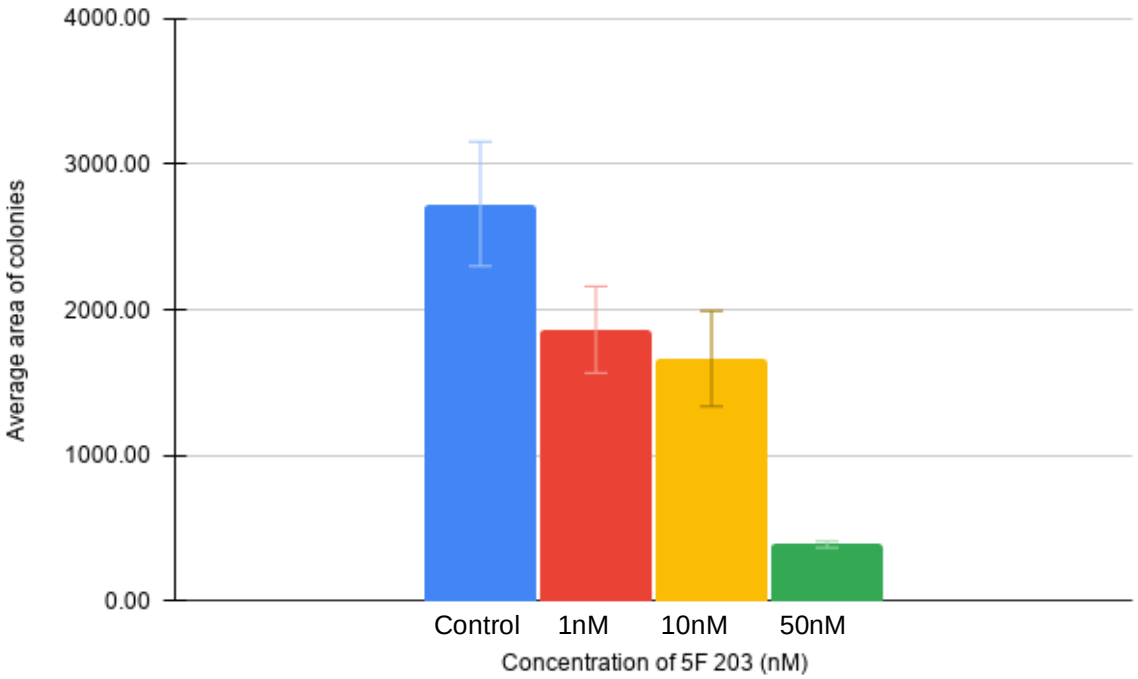

Figure 30: Clonogenic cell survival assay showing the effects of 5F 203 on colony formation with respect to the area of colonies. MCF-7 cells were seeded at a density of 250 cells per well, in 6 well plates and incubated overnight before treatment with 5F 203 at 1 nM, 10 nM and 50 nM for 24h. Cells were left for 6-8 days to form colonies, and then read when there were more than 50 cells in the control wells. Data points show mean and S.D. from one representative graph where internal repeats $n = 4$. Clonogenic plates provided by Dr Bradshaw for analysis.

Table 3: Summary of IC_{50} values from 4 independent clonogenic cell assays. *Data provided by T.D. Bradshaw, analysed by S. Duthoit. Mean IC_{50} value generated from 3 independent clonogenic experiments conducted by myself, and one conducted by Dr Bradshaw. Internal repeats *n=3.*

	Cell line and compound	
	MCF-7 5F 203 (nM) (number of colonies)	**MCF-7 5F 203 (nM) (area of colonies)**
IC_{50} values	31.88*	20.01*
	1.82	0.98
	2.17	1.33
	7.48	6.32
Mean IC_{50} value (± S.E.M.)	10.84 ± 7.13	7.17 ± 4.5

These results obtained align with the MTT data I obtained. The GI_{50} values for the MTT assays on MCF-7 and MDA-MB-468 cells were 7.42 nM and 6.42 nM respectively. Whilst there is a slight variation, these results are similar to the clonogenic assay results, confirming that 5F 203 causes potently inhibits growth and survival of breast cancer cells (known to possess inducible CYP1A1 enzyme) [67].

In clonogenic assays conducted, the brief exposure (24 h) to 5F 203 eliciting a cytotoxic response and inhibiting colony formation may be reflected clinically. This is because the body has evolved mechanisms to eliminate and detoxify xenobiotics and exposure of cancer cells to any drug is likely to be brief [122].

4.5 MCF-7 Tumourgenicity study

The following results I will be discussing were obtained from a tumourigenicity study conducted by collaborators in The School of Medicine, University of Nottingham. This study investigated the ability of MCF-7 cells to form tumours *in vivo*. It is the first in a series of *in vivo* experiments that include examination of i) MCF-7 tumourigenicity; ii)

AFt DDS tolerability and AFt-5F 203 tolerability; iii) pilot antitumour efficacy of AFt-5F 203.

Experiments have demonstrated *in vitro* that AFt is a non-toxic DDS [80] [103] [118]. It is important to establish the biocompatibility and non-toxicity of this DDS *in vivo* in tumour-bearing and non-tumour-bearing animals. It is also very important to establish that *in vitro* antitumour activity can translate to *in vivo* antitumour efficacy. In order to examine this hypothesis, we have sought to demonstrate that tumours, from the mammary cell line we use *in vitro*, will form in immune-deficient mice. To test this hypothesis, MCF-7 cell were transplanted either subcutaneously, (S.C.) or in the mammary fat pads (MFPs; more representative of human disease) of immune-deficient mice. It is necessary to use immune-deficient mice to allow for the transplantation of MCF-7 cells. If non immune-deficient mice were used, we would observe an immune response to the cancer cells, thus interfering with the results. Research *in vivo* can provide important information about a tumour microenvironment, and although tumour xenograft studies are more representative of human disease than *in vitro* research, it is important to remember that murine models are still not completely representative and shortcomings remain.

Both mean tumour volume and mean tumour diameter were monitored. The mean tumour volume and diameter was assessed over approximately 75 days. In comparison to *in vitro* assays (which are 72 hours long), this extensive time period provides vital information about the growth of tumours over an extended time period. This can be representative of the slow development of tumours in human cancer.

Results demonstrated that MCF-7 xenograft tumours could successfully be established in the flanks (s.c.) and MFPs of mice. Time-dependent increase in mean tumour volume and diameter was observed. For both cell types. The approximate time taken to double the mean tumour volume was 35 days (Figure 31), and the approximate time taken for the mean tumour diameter to double was 50 days (Figure 32). This slow and steady growth observed means that efficacy studies will be able to be tracked over a longer period of time, allowing for the monitoring of efficacy [123].

These results showed that in *in vivo* models, MCF-7 cells are capable of forming tumours. Following the completion of this tumourigenicity study, the next step will be to complete a tolerability study, to confirm that mice can tolerate varying concentrations of AFt and AFT-5F 203. This will indicate if murine models are suitable for the *in vivo* investigations into the encapsulation of 5F 203.

Previous research undergone has included the evaluation of the efficiency of Phortress (5F 203 lysylamide prodrug; Section 1.5.2) against eight independent carcinoma xenograft murine models (in comparison to the efficacy of doxorubicin). Research by Fichtner *et al* [124] found Phortress elicited significantly superior antitumour activity in comparison to doxorubicin in MCF-7 tumours. In these tumours, at doses of 12 and 18 mg/kg/injection, Phortress was able to induce significant tumour growth inhibition, whilst doxorubicin was unable to significantly influence tumour growth [124].

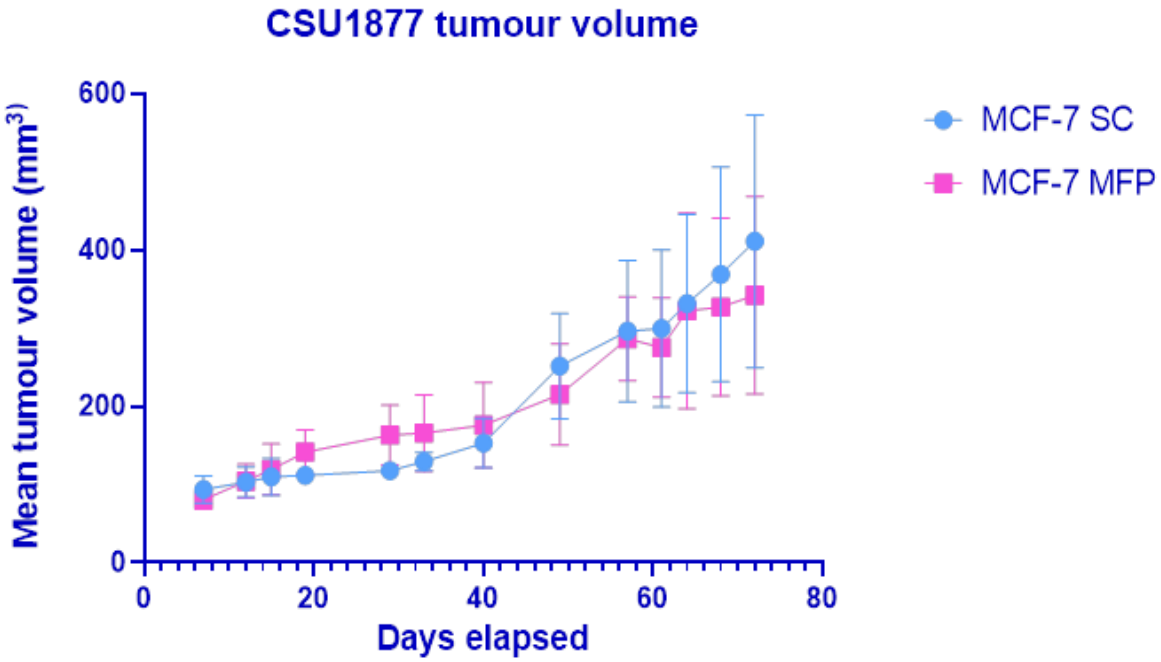

Figure 31: Graph showing the change in mean tumour volume of MCF-7 tumours with days elapsed**.** MCF-7 SC are tumours transplanted subcutaneously in the flank of the mouse, and MCF-7 MFP are tumours situated in the mammary fat pad.

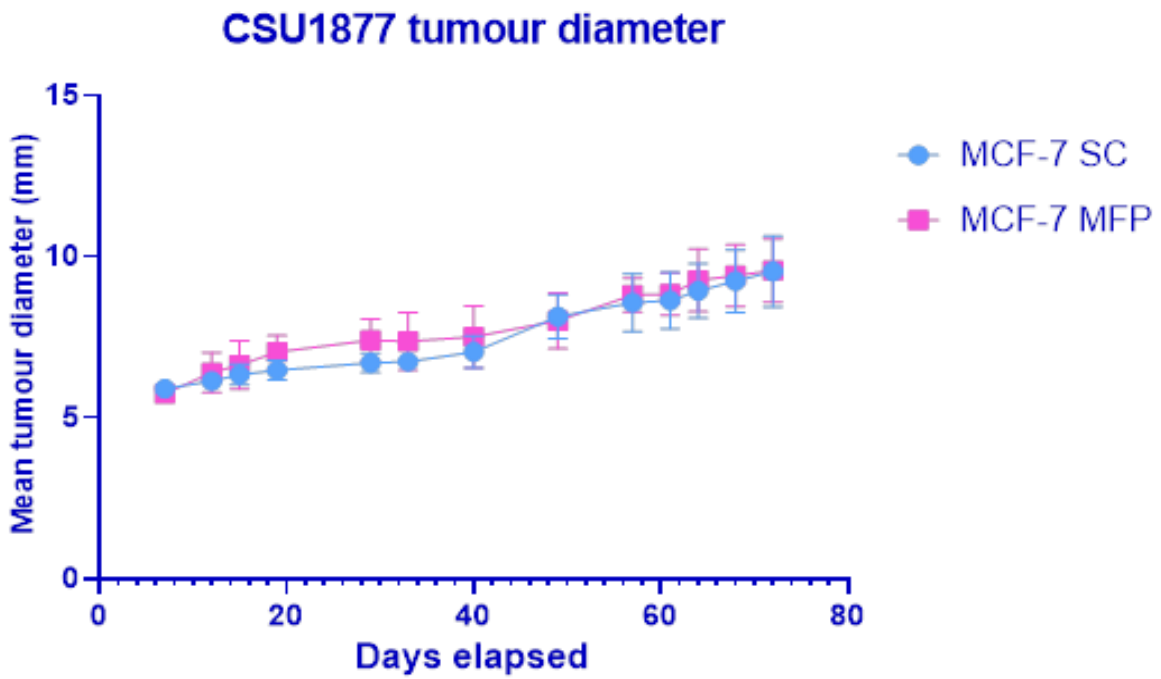

Figure 32: Graph showing the change in mean tumour diameter of MCF-7 tumours with days elapsed. MCF-7 SC are tumours transplanted subcutaneously in the flank of the mouse, and MCF-7 MFP are tumours situated in the mammary fat pad.

4.6 Conclusions and future research

4.6.1 Conclusion

In my research, I had originally aimed to encapsulate both 5F 203 and PbS QDs within AFt. Whilst this was not possible due to limitations imposed by the COVID-19 pandemic, significant progress has been made in the research of the therapeutic and imaging benefits of these compounds.

The results obtained show that 5F 203 evokes potent growth inhibitory effects on MCF-7 and MDA-MB-468 cell lines. 5F 203 elicited mean GI_{50} values of 7.42 nM and 6.43 nM in MCF-7 and MDA-MB-468 cell lines respectively. Therefore, the application of 5F 203 in the treatment of breast cancer that possesses inducible *cyp1a1* is very promising. (In addition to being activated by *cyp1a1*, research by Wang and Geungerich [125] and Tan *et al* [126] has shown that 5F 203 can be bioactivated by *cyp2w1*). 5F 203 can also be encapsulated in AFt to provide greater target selectivity,

due to the ability of AFt to target upregulated TfR1 receptors present on cancer cell surfaces [88]. We can conclude that it is beneficial to proceed with research into the AFt encapsulation of this compound.

The MTT studies conducted on PbS QDs have confirmed their cytotoxicity on MCF-7 cells, with an average GI_{50} value of 3.92 µg/mL. This cytotoxicity occurs due to the production of ROS by PbS QDs [127], meaning that it is important that they are encapsulated in a biocompatible DDS. In addition, PbS QDs can be absorbed into bones, which can lead to anaemia by inhibiting enzymes involved in the synthesis of the heme group [107].

It is possible to conclude that AFt is an suitable DDS, as previous research shows that it is biocompatible, biodegradable and non-immunogenic [92] [118]. Specifically, it is ideal to use in the treatment of breast cancer, as discussed, it targets the TFR1 that is commonly overexpressed on breast cancer cell surfaces [88]. The growth inhibition *in vitro* studies conducted confirm that AFt does not affect cell viability (Table 1). In addition, the PL spectra (Figure 20) of PbS QDs and AFt-PbS show that the gaps between the PL peaks and FQHM values are small, meaning that the protein cage structure is not changed after the addition of QDs. For this reason also, AFt provides a suitable delivery system for PbS QDs.

The DLS results confirm that the encapsulation of 5F 203 in AFt by diffusion did not affect protein integrity. In addition, the solution of reassembled AFt is stable and does not contain any particle aggregations. Research recently conducted by Haneen Abuzaid (manuscript under preparation), has found that AFt encapsulation of natural product jerantinine A *via* reassembly does not compromise the AFt capsule. Therefore, we can conclude that neither diffusion nor reassembly encapsulation techniques affect the structure or integrity of AFt.

I can conclude that AFt-encapsulated 5F 203 and PbS QDs are likely to offer a promising theranostic device, with potent and selective antitumour activity.

4.6.2 Future work

The findings of this project indicate the potential of 5F 203 and PbS QDs as part of a theranostic device in the treatment and diagnosis of breast cancer. The next step in the progression of this research would be to simultaneously encapsulate 5F 203 and PbS QDs in AFt. This would be possible, as the AFt cage could be dissembled/ reassembled in the initial encapsulation of PbS QDs (reassembly route). Following this, 5F 203 molecules could be introduced into the AFt cavity via nanoreactor encapsulation. In this method, 5F 203 passively diffuses through the hydrophobic and hydrophilic channels present in AFt. By following this order of encapsulation, both PbS QDs and 5F 203 could be entrapped within one AFt capsule.

Characterisation and optimisation

Following the successful encapsulation, the characterisation of AFt-PbS-5F 203 can be undertaken. The encapsulated nanoparticles can be characterised with DLS, native-PAGE, TEM and PL spectroscopy. TEM will be useful to ensure the encapsulation is successful, as it can be utilised to image AFt cages. DLS, native-PAGE and PL experiments will be useful to determine the size and integrity of the AFt nanoparticles. This will provide information about whether the simultaneous encapsulation of 5F 203 and PbS QDs alter the shape and size of the AFt nanoparticles, and whether compounds are entrapped within the AFt core, or attached to the exterior of the AFt capsule. A complementary technique, which could be adopted to further validate interior entrapment of 5F 203 is time of flight secondary ion mass spectrometry (ToFSIMS), as described by Breen et al [80].

Following the characterisation of the compound, the amount of 5F 203 and PbS QDs inside the AFt molecule can be determined via UV-vis spectroscopy and Bradford assays. The quantification of encapsulated molecules provides information about encapsulation efficiency and drug loading. Depending on the success of the encapsulation, further work may be required at this point to optimise the encapsulation of 5F 203 and PbS QDs in AFt cages.

In vitro activity of AFt-PbS QDs/ 5F 203

Following the successful encapsulation, the activity of AFt-PbS-5F 203 will be tested *in vitro*. To conduct this research, MCF-7 and MDA-MB-468 cell lines will be ideal, as

they express the inducible CYP 1A1 necessary for 5F 203 bioactivation. To analyse the *in vitro* activity, MTT assays, cell count assays and clonogenic assays can be utilised.

MTT assays will provide information on the metabolic activity of the cells. When MTT assays are conducted with AFt-PbS-5F 203**,** it will indicate the ability of cancerous cells to survive over a 72-hour time period. Cell count assays will also be conducted to corroborate MTT results, and rule out the possibility that activity detected in the MTT results was due to mitochondrial inhibition.

Whilst MTT and cell count assays can indicate the response of MCF-7 and MDA-MB-468 cells to the AFt-PbS QDs/ 5F 203 compound, we will also conduct clonogenic assays. These assays can indicate whether a compound causes a cytostatic or cytotoxic response to cells. To confirm the cancer-selective nature of the antitumour activity, the effects of AFt-PbS-5F 203 in non-tumourigenic MRC-5 fibroblasts should be examined. The selective growth inhibitory properties of 5F 203 and AFt-PbS QDs has been previously demonstrated [118] [103]. To confirm that the mechanism of action in MCF-7 and MDA-MB-468 cells is not perturbed by encapsulation, western blot assays should be conducted to detect CYP 1A1 protein in lysates of treated cells.

Based on the research detailed in Section 4, I hypothesise that the AFt-PbS-5F 203 composite would be cytotoxic to MCF-7 and MDA-MB-468 cancer cells, as individually both 5F 203 and PbS QDs elicited cancer-selective cytotoxicity against these mammary carcinoma cell lines.

In vitro imaging of AFt-PbS-5F 203

The next stage in the investigation of AFt-PbS-5F 203, will be to conduct *in vitro* imaging studies, to confirm that the diagnostic properties of the compound are as predicted.

Confocal microscopy will be undertaken to determine the intracellular update and distribution of 5F 203 and PbS QDs following the treatment of cells with AFt-PbS-5F 203. TEM can also be utilised to image the cells, and to indicate the integrity of AFt and presence of 5F 203 and QDs.

In vivo tolerability AFt-5F 203 and AFt-PbS-5F 203

Following completion of the *in vitro* work, *in vivo* evaluation should be undertaken. Whilst prior research [92] [118] has demonstrated that AFt is a non-toxic DDS *in vivo*, it is important to establish the biocompatibility and non-toxicity to healthy cells of AFt-PbS-5F 203. These experiments need to be conducted to confirm that murine models are able to tolerate varying concentrations of AFt-5F 203 and AFt-PbS-5F 203. Routinely, doses of test agent(s) are escalated until a maximum tolerated dose (MTD) is established. However, efficacious 5F 203 doses have already been established [64] [68] and therefore tolerability at these doses should be established and compared with naked agent.

In vivo efficacy AFt-5F 203 and AFt-PbS-5F 203

Efficacy studies serve the purpose of analysing the ability of a drug to inhibit tumour growth. We will conduct studies in murine models with MCF-7 tumours. Doses of AFt-PbS-5F 203 and AFt- 5F 203 will be administered intravenously (i.v.). As a result, we will be able to measure the ability of these compounds to inhibit tumour growth and /or cause tumour shrinkage. In addition, following treatment of mice with AFt-PbS-5F 203, we will be able to examine whether tumours can be imaged simultaneously.

In vivo imaging (efficacy) AFt-PbS QDS and AFt-PbS-5F 203

The study mentioned previously combines with PbS QDs with 5F 203 in a single AFt cage. We will conduct studies in mice bearing MCF-7 tumour xenografts. Similarly to the experiment detailed above, concentrations of AFt-PbS QDs/ 5F 203 will be administered i.v. to mice.

Varying concentrations of both AFt-PbS QDS and AFt-PbS-5F 203 will be injected into the mice, following which i*n vivo* fluorescent imaging can be utilised to image the 2nd-NIR-QDs, as detailed in [128]. Taking images periodically will be beneficial to provide information on the location of the compound. In addition to conducting NIR whole body

imaging, *ex vivo* tissue sections will also be imaged, to provide valuable information about the locations of the PbS QDs and 5F 203.

These experiments will guide selection of required concentrations of AFt-PbS-5F 203 required for optimal tumour imaging and therapy.

Chapter 5: References

1. UK, C.R. *Cancer statistics for the UK*. 2020; Available from: https://www.cancerresearchuk.org/health-professional/cancer-statistics-for-the-uk.
2. UK, C.R. *How chemotherapy works*. 2017 [cited 2020 29 April]; Available from: https://www.cancerresearchuk.org/about-cancer/cancer-in-general/treatment/chemotherapy/how-chemotherapy-works.
3. Kilic, M.A., E. Ozlu, and S. Calis, *A novel protein-based anticancer drug encapsulating nanosphere: apoferritin-doxorubicin complex.* Journal of Biomedical Nanotechnology, 2012. **8**(3): p. 508-514.
4. WHO. *Cancer*. 2018 [cited 2020 29 April]; Available from: https://www.who.int/en/news-room/fact-sheets/detail/cancer.
5. UK, C.R. *Breast cancer statistics*. [cited 2020 29 November]; Available from: https://www.cancerresearchuk.org/health-professional/cancer-statistics/statistics-by-cancer-type/breast-cancer.
6. Downward, J., *Cell cycle: Routine role for Ras.* Current Biology, 1997. **7**(4): p. R258-R260.
7. Burstein, H., *The distinctive nature of HER2-positive breast cancers.* N Engl J Med, 2005. **353**(16): p. 1652-1654.
8. Slamon, D., et al., *Human Breast Cancer: Correlation of Relapse and Survival with Amplification of the HER-2/neu Oncogene.* Science, 1987. **235**(4785): p. 177-182.
9. Hanahan, D. and R. Weinberg, *Hallmarks of Cancer: The Next Generation.* Cell, 2011. **144**(5): p. 646-674.
10. Cancer.org. *Oncogenes and tumor suppressor genes*. 2014 [cited 2020 16th December]; Available from: https://www.cancer.org/cancer/cancer-causes/genetics/genes-and-cancer/oncogenes-tumor-suppressor-genes.html.
11. (US)., N.C.f.B.I., *Genes and Disease*. 1998.
12. Toufektchan, E. and F. Toledo, *The Guardian of the Genome Revisited: p53 Downregulates Genes Required for Telomere Maintenance, DNA Repair, and Centromere Structure.* Cancers, 2018. **10**(5).
13. Hanahan, D. and R. Weinberg, *The Hallmarks of Cancer.* Cell, 2000. **100**(1): p. 57-70.
14. GM, C., *The Cell: A Molecular Approach*. 2nd ed. 2000.
15. OpenStax College, B. *Control of the cell cycle*. [cited 2020 29 November]; Available from: https://cnx.org/contents/GFy_h8cu@14.1:abji7vNQ@8/10-3-Control-of-the-Cell-Cycle.
16. Souza, C.P.C.D. and S.A. Osmani, *Mitosis, not just open or closed.* Eukaryotic Cell, 2017.
17. Elledge, S., *Cell Cycle Checkpoints: Preventing an Identity Crisis.* Science, 1996. **274**(5293): p. 1664-1672.
18. Majc, B., et al., *Epithelial-to-mesenchymal transition as the driver of changing carcinoma and glioblastoma microenvironment.* Biochimica et Biophysica Acta - Molecular Cell Research, 2020. **10**.
19. Beffy, P., et al., *Altered signal transduction pathways and induction of autophagy in human myotonic dystrophy type 1 myoblasts.* The International Journal of Biochemistry & Cell Biology, 2010.

20. Gutierrez, C. and R. Schiff, *HER 2: Biology, Detection, and Clinical Implications.* Archives of Pathology & Laboratory Medicine, 2011. **135**(1): p. 55-62.
21. Libson, S. and M. Lippman, *A review of clinical aspects of breast cancer.* International Review of Psychiatry, 2014. **26**(1): p. 4-15.
22. Kumar, B., et al., *Normal Breast-Derived Epithelial Cells with Luminal and Intrinsic Subtype-Enriched Gene Expression Document Interindividual Differences in Their Differentiation Cascade.* Cancer Research Translational Science, 2018. **78**(17).
23. Amin, A.R.M.R., et al., *Evasion of anti-growth signaling: a key step in tumorigenesis and potential target for treatment and prophylaxis by natural compounds*

Seminal Cancer Biology, 2015. **35**: p. S55-S77.
24. Shammas, M.A., *Telomeres, lifestyle, cancer, and aging.* Curr Opin Clin Nutr Metab Care., 2012. **14**(1): p. 28-34.
25. Viti, M.D., F. Berardinelli, and A. Sgura, *Telomere Length Maintenance in Cancer: At the Crossroad between Telomerase and Alternative Lengthening of Telomeres (ALT).* International journal of Molecular Sciences, 2018. **19**(2): p. 606.
26. Adair, T. and J. Montani, *Angiogensis.* 2010: Morgan and Claypool life sciences.
27. Bielenberg, D.R. and B.R. Zetter, *The Contribution of Angiogenesis to the Process of Metastasis.* Cancer, 2016. **21**(4): p. 267-273.
28. Nishida, N., et al., *Angiogenesis in Cancer.* Vascular Health and Risk Management, 2006. **2**(3): p. 213-219.
29. Roy, S.S. and R.K. Vadlamudi, *The Influence of the Cancer Microenvironment on the Process of Metastasis.* International journal of Breast Cancer, 2011. **2012**: p. 8.
30. Peng, F., et al., *Nanoparticles promote in vivo breast cancer cell intravasation and extravasation by inducing endothelial leakiness.* Nature Nanotechnology, 2019. **14**.
31. Fernald, K. and M. Kurokawa, *Evading apoptosis in cancer.* Trends in Cell Biology, 2013. **23**(12): p. 620-633.
32. Fulda, S., *Evasion of Apoptosis as a Cellular Stress Response in Cancer.* International Journal of Cell Biology, 2009. **2010**.
33. Westphal, D., R.M. Kluck, and G. Dewson, *Building blocks of the apoptotic pore: how Bax and Bak are activated and oligomerize during apoptosis.* Cell Death and Differentiation, 2014. **21**: p. 196-205.
34. Anastasiadi, Z., et al., *Breast cancer in young women: an overview.* Updates in Surgery, 2017. **69**: p. 313-317.
35. Cancer.org. *What is Breast Cancer?* 2019 [cited 2020 19th December].
36. Perou, C.M., et al., *Molecular portraits of human breast tumours.* Nature, 2000. **406**: p. 747-752.
37. Taherian-Fard, A., S. Srihari, and M.A. Ragan, *Breast cancer classification: linking molecular mechanisms to disease prognosis. .* Briefings in Bioiformatics, 2014. **16**(3): p. 461-474.
38. Cancer.org. *Breast Cancer Hormone Receptor Status*. 2019; Available from: https://www.cancer.org/cancer/breast-cancer/understanding-a-breast-cancer-diagnosis/breast-cancer-hormone-receptor-status.html.
39. Harbeck, N. and M. Gnant, *Breast Cancer.* The Lancet, 2017. **389**(10074): p. 1134-1150.
40. Vuong, D., et al., *Molecular classification of breast cancer.* Virchows Arch, 2014. **465**(1): p. 1-14.
41. Zhao, C., K. Dahlman-Wright, and J.-Å. Gustafsson, *Estrogen receptor β: an overview and update.* Nuclear Receptor Signalling 2008. **6**.

42. Fan, P., et al., *The Molecular, Cellular and Clinical Consequences of Targeting the Estrogen Receptor Following Estrogen Deprivation Therapy. .* Molecular and Cellular Endocrinology, 2015. **418**(3): p. 245-263.
43. Rajbhandari, P., et al., *Regulation of Estrogen Receptor α N-Terminus Conformation and Function by Peptidyl Prolyl Isomerase Pin1.* Molecular and Cellular Biology, 2012. **32**(2): p. 445-457.
44. Williams, C. and C.-Y. Lin, *Oestrogen receptors in breast cancer: basic mechanisms and clinical implications.* Cancer medical science. **7**(370).
45. Hua, H., et al., *Mechanisms for estrogen receptor expression in human cancer.* Experimental Hematology and Oncology, 2018. **7**.
46. Carroll, J.S., *Mechanisms of oestrogen receptor (ER) gene regulation in breast cancer.* European Journal of Endocrinology, 2016. **175**(1): p. R41-R49.
47. Kim, J.J., T. Kurita, and S.E. Bulun, *Progesterone Action in Endometrial Cancer, Endometriosis, Uterine Fibroids, and Breast Cancer.* Endocrine Reviews, 2013. **34**(1).
48. Diep, C.H., et al., *Progesterone action in breast, uterine, and ovarian cancers. .* J Mol Endocrinol., 2015. **54**(2): p. 31-53.
49. Richer, J.K., et al., *Differential Gene Regulation by the Two Progesterone Receptor Isoforms in Human Breast Cancer Cells.* Journal of Biological Chemistry, 2002. **227**(7).
50. Escrivá-de-Romaní, S., et al., *HER2-positive breast cancer: Current and new therapeutic strategies.* The Breast, 2018. **39**: p. 80-88.
51. Jerusalem, G., P. Lancellotti, and S.-B. Kim, *HER2+ breast cancer treatment and cardiotoxicity: monitoring and management.* Breast Cancer Research and Treatment, 2019. **117**(2): p. 237-250.
52. Breastcancer.org. *HER2 Status: Tests, Treatments, And More. .* 2020 [cited 2020; Available from: https://www.breastcancer.org/symptoms/diagnosis/her2.
53. Steelman, L.S., et al., *Roles of the Raf/MEK/ERK and PI3K/PTEN/Akt/mTOR pathways in controlling growth and sensitivity to therapy-implications for cancer and aging.* Aging, 2011. **3**(3): p. 192-222.
54. Bianchini, G., et al., *Triple-negative breast cancer: challenges and opportunities of a heterogeneous disease.* Nature Reviews Clinical Oncology, 2016. **13**(11): p. 674-690.
55. Hayes, D.F., et al., *HER2 and response to paclitaxel in node-positive breast cancer.* The New England Journal of Medicine, 2007. **357**(15).
56. Perez-Verdia, A., et al., *Acute Cardiac Toxicity Associated with High-Dose Intravenous Methotrexate Therapy: Case Report and Review of the Literature.* American College of Clinical Pharmacy, 2012.
57. Wang, X.H., et al., *Design, synthesis, and biological activity evaluation of campthothecin-HAA-Norcantharidin conjugates as antitumor agents in vitro.* Chemical Biology & Drug Design, 2018.
58. D, G., et al., *Taxane-containing regimens for metastatic breast cancer.* Cochrane, 2015.
59. Secreto, G. and B. Zumoff, *Role of Androgen Excess in the Development of Estrogen Receptor-positive and Estrogen Receptor-negative Breast Cancer.* Anticancer Research 2012. **2012**(32): p. 8.
60. Nagini, S., *Breast Cancer: Current Molecular Therapeutic Targets and New Players.* Anti-Cancer Agents in Medicinal Chemistry, 2017. **17**(2): p. 152-163.
61. Sharma, P.C., et al., *Medicinal significance of benzothiazole scaffold: an insight view. .* Journal of Enzyme Inhibition and Medicinal Chemistry, 2012. **28**(2): p. 240-266.

62. Singh, M., et al., *Design, synthesis and mode of action of some benzothiazole derivatives bearing an amide moiety as antibacterial agents.* RSC Advances, 2014. **4**(36): p. 19013-19023.
63. Akhtar, T., et al., *In vitro antitumor and antiviral activities of new benzothiazole and 1,3,4-oxadiazole-2-thione derivatives.* Acta Pharmaceuticals, 2008. **58**(2): p. 135-149.
64. Bradshaw, T., et al., *2-(4-Aminophenyl)benzothiazoles: novel agents with selective profiles of in vitro anti-tumour activity.* Br J Cancer, 1998. **77**(5): p. 745-752.
65. Bradshaw, T., *Phortress: the smart antitumour agent which induces its own metabolism.* The Pharmaceutical Journal, 2010.
66. Callero, M. and A. Perez, *The Role of Aryl Hydrocarbon Receptor and Crosstalk with Estrogen Receptor in Response of Breast Cancer Cells to the Novel Antitumor Agents Benzothiazoles and Aminoflavone.* International Journal of Breast Cancer, 2011. **4**.
67. Chua, M.S., et al., *Role of CYP1A1 in Modulation of Antitumor Properties of the Novel Agent 2-(4-Amino-3-methylphenyl)benzothiazole (DF 203, NSC 674495) in Human Breast Cancer Cells.* Cancer Research, 2000. **60**(18).
68. Bradshaw, T.D., M.F.G. Stevens, and A.D. Westwell, *The Discovery of the Potent and Selective Antitumour Agent 2-(4-Amino-3-methylphenyl)benzothiazole (DF 203) and Related Compounds.* Current Medicinal Chemistry, 2001. **8**(2): p. 203-210.
69. T.D., B., et al., *Preclinical Toxicokinetic Evaluation of Phortress [2-(4-Amino-3-Methylphenyl)-5-Fluorobenzothiazole Lysylamide Dihydrochloride] in Two Rodent Species.* Pharmacology, 2009. **93**: p. 99-109.
70. NIH. *Drug Delivery Systems*. 2016 [cited 2020 16th OCtober]; Available from: https://www.nibib.nih.gov/science-education/science-topics/drug-delivery-systems-getting-drugs-their-targets-controlled-manner#pid-1236
71. Jain, V., *Nanomedicines based drug delivery systems for anti-cancer targeting and treatment* Current Drug Delivery, 2015. **12**(2).
72. Attia, M.F., et al., *An overview of active and passive targeting strategies to improve the nanocarriers efficiency to tumour sites.* Journal of Pharmacy and Pharmacology, 2019. **71**(8).
73. Therapeutics, B., *A Study of BIND-014 in Patients With Urothelial Carcinoma, Cholangiocarcinoma, Cervical Cancer and Squamous Cell Carcinoma of the Head and Neck (iNSITE2)*. 2015: ClinicalTrials.gov.
74. Kolate, A., et al., *PEG - a versatile conjugating ligand for drugs and drug delivery systems.* Journal of Controlled Release, 2014. **28**(192): p. 67-81.
75. Suk, J.S., et al., *PEGylation as a strategy for improving nanoparticle-based drug and gene delivery.* Advanced Drug Delivery Reviews, 2016: p. 28-51.
76. Senapati, S., et al., *Controlled drug delivery vehicles for cancer treatment and their performance.* Signal Transduction and Targeted Therapy, 2018(7).
77. P. ANITHA, et al., *Recent Progress of Dendrimers in Drug Delivery for Cancer Therapy.* International journal of applied pharmaceutics, 2018. **10**(5).
78. Choudhary, S., L. Gupta, and U. Gupta, *Impact of Dendrimers on Solubility of Hydrophobic Drug Molecules.* Frontiers in Pharmacology, 2017. **8**(261).
79. Quintana, A., et al., *Design and Function of a Dendrimer-Based Therapeutic Nanodevice Targeted to Tumor Cells Through the Folate Receptor.* Pharmaceutical Research, 2002. **19**.

80. Breen, A.F., et al., *Development of novel apoferritin formulations for antitumour benzothiazoles.* Cancer Reports, 2019.
81. Ja, D., et al., *Protein-Based Drug-Delivery Materials.* Materials, 2017. **10**(5).
82. Sripriyalakshmi, S., *Recent Trends in Drug Delivery System Using Protein Nanoparticles.* Cell Biochemistry and Biophysics, 2014. **70**(17-26).
83. Friess, W., *Collagen – biomaterial for drug delivery.* European Journal of Pharmaceutics and Biopharmaceutics, 1998.
84. Hurrell, R. and R. Kelishadi, *Review on iron and its importance for human health.* J Res Med Sci, 2014. **19**(2): p. 164-174.
85. Sazanov, L.A. and P. Hinchliffe, *Structure of the Hydrophilic Domain of Respiratory Complex I from Thermus thermophilus.* Science, 2006. **311**(5766): p. 1430-1436.
86. Cheney, K., et al., *Survival after a severe iron poisoning treated with intermittent infusions of deferoxamine.* Journal of Toxicology: Clinical Toxicology, 1995. **33**(1): p. 61-66.
87. University, W. *Iron in Biology: Study of the Iron Content in Ferritin, The Iron-Storage Protein.* 2000 [cited 2020 21 December]; Available from: http://www.chemistry.wustl.edu/~edudev/LabTutorials/Ferritin/Ferritin.html.
88. Shen, Y., *Transferrin receptor 1 in cancer: a new sight for cancer therapy.* Am J Cancer Res, 2018. **8**(6): p. 916-931.
89. Nakamura, T., I. Naguro, and H. Ichijo, *Iron homeostasis and iron-regulated ROS in cell death, senescence and human diseases.* Biochimica et Biophysica Acta, 2019. **1863**(9): p. 1398-1409.
90. Crichton, R.R. and C. Charloteaux-Wauters, *Iron transport and storage.* Eur J Biochem, 1987. **168**(3): p. 485-506.
91. Crichton, R.R., *A role for ferritin in the regulation of iron metabolism.* FEBS Letters, 1973. **34**(2): p. 125.
92. Kuruppu, A.I., et al., *An Apoferritin-based Drug Delivery System for the Tyrosine Kinase Inhibitor Gefitinib.* Advanced healthcare materials, 2015.
93. Bouzinab, K., et al., *Abstract 1727: Challenging resistance to temozolomide in glioblastoma by drug encapsulation in apoferritin.* Cancer Research, 2020. **80**(16).
94. Kelkar, S.S. and T.M. Reineke, *Theranostics: Combining Imaging and Therapy.* Bioconjugate Chemistry, 2011. **22**(10): p. 1879-1903.
95. Jeelani, S., et al., *Theranostics: A treasured tailor for tomorrow.* Journal of Pharmacy and BioAllied Sciences, 2014. **6**(5): p. 6-8.
96. Alberti, C., *From molecular imaging in preclinical/clinical oncology to theranostic applications in targeted tumor therapy.* European Review for Medical and Pharmacological Sciences, 2012. **16**: p. 1925-1933.
97. Lu, P.J. and D.A. Weitz, *Colloidal Particles: Crystals, Glasses, and Gels. .* Annual Review of Condensed Matter Physics, 2013. **4**: p. 217-233.
98. Walling, M.A., J.A. Novak, and J.R.E. Shepard, *Quantum Dots for Live Cell and In Vivo Imaging.* International journal of Molecular Sciences, 2009. **10**(2).
99. Display, S. *Quantum dot physics: A guide to understanding QD displays* 2020 [cited 2021 23rd February]; Available from: https://pid.samsungdisplay.com/en/learning-center/white-papers/guide-to-understanding-quantum-dot-displays.
100. Brunetti, J., et al., *Near-infrared quantum dots labelled with a tumor selective tetrabranched peptide for in vivo imaging.* Journal of Nanobiotechnology, 2018. **16**(21).

101. Liu, H., et al., *Magnetic-induced graphene quantum dots for imaging-guided photothermal therapy in the second near-infrared window.* Biomaterials, 2020. **232**.
102. Turyanska, L., et al., *The differential effect of apoferritin-PbS nanocomposites on cell cycle progression in normal and cancerous cells.* Journal of Materials Chemistry, 2012. **22**(2): p. 660-665.
103. Bradshaw, T.D., *Apoferritin-encapsulated PbS quantum dots significantly inhibit growth of colorectal carcinoma cells. .* Journal of Materials Chemistry, 2013. **1**: p. 6254-6260.
104. Michalet, X., et al., *Quantum Dots for Live Cells, in Vivo Imaging, and Diagnostics.* Science, 2005. **307**(5709): p. 538-544.
105. Zamberlan, F., et al., *Stable DHLA–PEG capped PbS quantum dots: from synthesis to near-infrared biomedical imaging.* Journal of Materials Chemistry, 2018(4).
106. Dai, X., et al., *Breast Cancer Cell Line Classification and Its Relevance with Breast Tumor Subtyping.* Journal of Cancer, 2017. **8**(16): p. 3131-3141.
107. Hennequin, B., et al., *Aqueous Near-Infrared Fluorescent Composites Based on Apoferritin-Encapsulated PbS Quantum Dots.* Advanced Materials, 2008.
108. Rames, M., Y. Yu, and G. Ren, *Optimized negative staining: a high-throughput protocol for examining small and asymmetric protein structure by electron microscopy.* Journal of Visualized Experiments, 2014. **90**.
109. ATTC. *MCF7 (ATCC® HTB-22™)*. 2020 [cited 2020 30/12]; Available from: https://www.lgcstandards-atcc.org/products/all/htb-22.aspx?geo_country=gb#generalinformation.
110. ATTC. *MDA-MB-468 (ATCC® HTB-132™)*. 2020 [cited 2021 5th January]; Available from: https://www.lgcstandards-atcc.org/products/all/HTB-132.aspx#generalinformation.
111. Sigmaaldrich. *Protocol Guide: MTT Assay for Cell Viability and Proliferation*. 2020 [cited 2021 5th January]; Available from: https://www.sigmaaldrich.com/technical-documents/protocols/biology/roche/cell-proliferation-kit-i-mtt.html.
112. Puck, T. and P. Marcus, *Action of x-rays on mammalian cells.* Journal of Experimental Medicine 1956. **103**(5).
113. Franken, N.A.P., et al., *Clonogenic assay of cells in vitro.* Nature, 2006. **1**: p. 2315-2319.
114. Munshi, A., M. Hobbs, and R.E. Meyn, *Clonogenic cell survival assay.* Methods in Molecular Medicine, 2005. **110**: p. 21-28.
115. Buch, K., et al., *Determination of cell survival after irradiation via clonogenic assay versus multiple MTT Assay - A comparative study.* Radiation Oncology, 2012.
116. Rodarte, A.L., et al., *Quantum Dot/Liquid Crystal Nanocomposites in Photonic Devices.* Photonics, 2015. **2**.
117. Takeda, S., et al., *Control of crystal forms of apoferritin by site-directed mutagenesis.* Proteins, 1995. **23**(4).
118. Turyanska, L., et al., *The biocompatibility of apoferritin-encapsulated PbS quantum dots.* Small, 2009. **3**(5).
119. N.Petsev, D., et al., *Interactions and Aggregation of Apoferritin Molecules in Solution: Effects of Added Electrolytes.* Biophysical Journal, 2000. **78**(4).
120. Wang, K. and F.P. Guengerich*, *Bioactivation of Fluorinated 2-Aryl-benzothiazole Anti-tumor Molecules by Human Cytochrome P450s 1A1 and 2W1 and Deactivation by Cytochrome P450 2S1.* Chemical research in toxicology, 2012. **25**(8).

121. Wang, Y., et al., *The antitumour activity of 2-(4-amino-3-methylphenyl)-5-fluorobenzothiazole in human gastric cancer models is mediated by AhR signalling.* Journal of Cellular and Molecular Medicine, 2020. **24**.
122. Croom, E., *Chapter Three - Metabolism of Xenobiotics of Human Environments.* Progress in Molecular Biology and Translational Science, 2012. **112**: p. 31-88.
123. Newell, H. and E. Sausville, *Cytotoxic drugs: past, present and future.* Cancer chemotherapy and pharmacology, 2016. **77**.
124. Fichtner, I., et al., *The experimental antitumor agents Phortress and Doxorubicin are equiactive against human-derived breast carcinoma xenograft models.* Breast Cancer Research and Treatment, 2004. **87**: p. 97-107.
125. Wang, K. and F.P. Guengerich, *Bioactivation of Fluorinated 2-Aryl-benzothiazole Antitumor Molecules by Human Cytochrome P450s 1A1 and 2W1 and Deactivation by Cytochrome P450 2S1.* Chemical research in toxicology, 2012. **25**(8).
126. Tan, B.S., et al., *CYP2S1 and CYP2W1 mediate 2-(3,4-dimethoxyphenyl)-5-fluorobenzothiazole (GW-610, NSC 721648) sensitivity in breast and colorectal cancer cells.* Molecular cancer therapeutics, 2011. **10**(10).
127. Zhu, C., et al., *Recent advances in non-toxic quantum dots and their biomedical applications.* Progress in Natural Science: Materials International, 2019. **29**(6).
128. Imamura, Y., *Applications of Highly Bright PbS Quantum Dots to Non-Invasive Near-Infrared Fluorescence Imaging in the Second Optical Window.* ECS Journal of Solid State Science and Technology, 2016. **5**(1).